Society for Endocrinology
ENDOCRINE-RELATED CANCER

Transcriptomic landscape of radiation-induced murine thyroid proliferative lesions

Journal:	*Endocrine-Related Cancer*
Manuscript ID	ERC-21-0019
Manuscript Type:	Research Paper
Date Submitted by the Author:	14-Jan-2021
Complete List of Authors:	Stauffer, Elena; Helmholtz Center Munich German Research Center for Environmental Health, Research Unit of Radiation Cytogenetics Weber, Peter; Helmholtz Center Munich German Research Center for Environmental Health, Research Unit of Radiation Cytogenetics Heider, Theresa; Helmholtz Center Munich German Research Center for Environmental Health, Research Unit of Radiation Cytogenetics Dalke, Claudia; Helmholtz Center Munich German Research Center for Environmental Health, Institute for Metabolism and Cel Death Blutke, Andreas; Helmholtz Center Munich German Research Center for Environmental Health, Research Unit Analytical Pathology Walch, Axel; Helmholtz Center Munich German Research Center for Environmental Health, Research Unit Analytical Pathology Lauber, Kirsten; LMU, Department of Radiation Oncology Brix, Nikko; LMU, Department of Radiation Oncology Burgstaller, Gerald; Helmholtz Center Munich German Research Center for Environmental Health, Institute of Lung Biology and Disease Zitzelsberger, Horst; Helmholtz Center Munich German Research Center for Environmental Health, Research Unit of Radiation Cytogenetics Unger, Kristian; Helmholtz Center Munich German Research Center for Environmental Health, Research Unit of Radiation Cytogenetics Selmansberger, Martin; Helmholtz Center Munich German Research Center for Environmental Health, Research Unit of Radiation Cytogenetics
Keywords:	Carcinogenesis, Transcriptomic profiling, Thyroid proliferative lesions

Transcriptomic landscape of radiation-induced murine thyroid proliferative lesions

Elena Stauffer[a], Peter Weber[a], Theresa Heider[a], Claudia Dalke[b], Andreas Blutke[c], Axel Walch[c], Gerald Burgstaller[d], Nikko Brix[e], Kirsten Lauber[e,f], Horst Zitzelsberger[a,f], Kristian Unger[a,e,f,*] and Martin Selmansberger[a,*,§]

[a] Helmholtz Zentrum München - German Research Center for Environmental Health, Research Unit Radiation Cytogenetics, Neuherberg, Germany

[b] Helmholtz Zentrum München - German Research Center for Environmental Health, Institute of Metabolism and Cell Death, Neuherberg, Germany

[c] Helmholtz Zentrum München - German Research Center for Environmental Health, Research Unit Analytical Pathology, Neuherberg, Germany

[d] Helmholtz Zentrum München - Institute of Lung Biology and Disease (ILBD) and Comprehensive Pneumology Center (CPC), Member of the German Center for Lung Research (DZL), Munich, Germany

[e] Department of Radiation Oncology, University Hospital, LMU Munich, Munich, Germany

[f] Helmholtz Zentrum München - German Research Center for Environmental Health GmbH, Clinical Cooperation Group "Personalized Radiotherapy in Head and Neck Cancer", Neuherberg, Germany.

[*] These authors contributed equally to this paper.

[§] Corresponding author

Elena Stauffer: elena.stauffer@helmholtz-muenchen.de

Dr. Peter Weber: peter.weber@helmholtz-muenchen.de

Theresa Heider: theresa.heider@helmholtz-muenchen.de

Dr. Claudia Dalke: dalke@helmholtz-muenchen.de

Dr. Andreas Blutke: andreas.parzefall@helmholtz-muenchen.de

Prof. Dr. Axel Walch: axel.walch@helmholtz-muenchen.de

Dr. Gerald Burgstaller: gerald.burgstaller@helmholtz-muenchen.de

Dr. Nikko Brix: nikko.brix@med.uni-muenchen.de

Prof. Dr. Kirsten Lauber: kirsten.lauber@med.uni-muenchen.de

Prof. Dr. Horst Zitzelsberger: zitzelsberger@helmholtz-muenchen.de

Dr. Kristian Unger: unger@helmholtz-muenchen.de

Dr. Martin Selmansberger: martin.selmansberger@helmholtz-muenchen.de

Helmholtz Zentrum Muenchen

Ingolstäter Landstrasse 1

85764 Oberschleißheim, Germany

Short title: Transcriptomics of early-state thyroid proliferative lesions

Keywords: thyroid pathogenesis, thyroid carcinogenesis, thyroid neoplasia, histology, transcriptomics

ABSTRACT

Thyroid carcinoma incidence rates in western societies are among the fastest rising, compared to all malignant tumors over the past two decades. While risk factors such as age and exposure to ionizing radiation are known, early-state carcinogenic processes or pre-lesions are poorly understood or unknown. This study aims at the identification and characterization of early-state radiation-associated neoplastic processes by histologic and transcriptomic analyses of thyroid tissues derived from a mouse model. Comprehensive histological examination of 246 thyroids (164 exposed, 82 non-exposed) was carried out. Proliferative and normal tissues from exposed cases and normal tissue from non-exposed cases were collected by laser-capture microdissection, followed by RNAseq transcriptomic profiling using a low input 3`-library preparation protocol, differential gene expression analysis and functional association by *Gene Set Enrichment Analysis*. Nine exposed samples exhibited proliferative lesions, while none of the non-exposed samples showed histological abnormalities, indicating an association of ionizing radiation exposure with histological abnormalities. Activated immune response signaling and deregulated metabolic processes were observed in irradiated tissue with normal histology compared to normal tissue from non-exposed samples. Proliferative lesions compared to corresponding normal tissues showed enrichment for mainly proliferation-associated gene sets. Consistently, proliferative lesion samples from exposed mice showed elevated proliferation-associated signaling and deregulated metabolic processes compared to normal samples from non-exposed mice. Our findings indicate that a molecular deregulation is already detectable in histologically normal thyroid

tissues and in early proliferative lesions in the frame of multi-step progression from irradiated normal tissue to tumorous lesions.

Words: 243

INTRODUCTION

Incidence rates for thyroid cancer increased worldwide over the last decades, thus becoming the most common endocrine malignancy (La Vecchia et al., 2015). While environmental and lifestyle factors and the effect of overdiagnosis due to improved screening methods are discussed, their impact on the increased incidence rates remains to be proved (Wiltshire et al., 2016). Despite the high incidence rates, thyroid cancer, especially the papillary thyroid carcinoma (PTC) subtype, is associated with a good prognosis after radical surgery and shows low mortality rates (La Vecchia et al., 2015).

Exposure to ionizing radiation at young age, both internal and external, is a well-known risk factor for the development of thyroid carcinoma (Ron et al., 1995). Ionizing radiation exposure in childhood greatly increases the risk for thyroid cancer, particularly PTC. Numerous studies have shown that after the Chernobyl reactor accident and the resulting radiation exposure of the population through radioactive fallout (including I-131), the incidence rate of thyroid carcinomas has significantly increased (Efanov et al., 2018, Cahoon et al., 2017, Nikiforov, 2006, Kazakov et al., 1992).

Thyroid carcinomas can develop either from follicular cells or c-cells. The resulting malignancies are classified into medullary carcinomas (c-cells) or papillary, follicular and anaplastic carcinomas (follicular cells). Papillary carcinomas are further divided into different subtypes based on the predominant histological architecture (Xing, 2013). The majority of thyroid cancer originates from follicular cells such as PTC and follicular thyroid carcinoma (FTC) (Baloch and LiVolsi, 2018, DeLellis RA, 2004). While

it is proposed that FTC evolves from follicular adenoma (FA), papillary thyroid carcinoma has no benign precursor lesion (Sponziello et al., 2013).

Mouse models are frequently used to study thyroid cancer and the underlying carcinogenic processes. However, although mouse and human thyroid cancers show biological similarities, they greatly differ in histological characteristics. In contrast to human thyroid cancer, murine histological cancer entities are not distinguished, e.g. the follicular carcinoma has only a papillary pattern but is classified as follicular carcinoma (Capen, 2001, Boorman G A, 1995).

As for other cancer types, a series of genetic and epigenetic alterations is responsible for initiation and progression of thyroid cancer according to a multi-step model (Kondo et al., 2006, Vogelstein and Kinzler, 1993). Those alterations, that consequently stimulate effectors of the MAPK signaling pathway or PI3K/AKT signaling pathway, play a central role in thyroid carcinogenesis (Nikiforova and Nikiforov, 2008). Point mutation of the BRAF and RAS genes and rearrangements of the RET gene are common in PTC, while the rearrangements of PAX8/PPARγ are mostly prevalent in FTC and FTA (Nikiforov and Nikiforova, 2011, Xing, 2005). The detection of genetic alterations in follicular adenoma, which can be considered as early lesions, support the concept of a multi-step carcinogenesis model. However, it remains unclear at what point follicle cells develop proliferative potential (Jung et al., 2016). Additionally, a cancer stem cell carcinogenic model and a fetal cell carcinogenesis model are currently discussed as alternatives to the multi-step process (Zane et al., 2016).

Nowadays, molecular alterations in thyroid cancer are well characterized, while early state events or precursor lesions still remain poorly understood or are unknown (Ye et al., 2017, Xing, 2013). Besides genetic aberrations such as RET- and PAX8-

rearrangements and BRAF V600E mutations, epigenetic modifications including silencing of RASSF1A via promoter methylation and post-transcriptional regulation via miRNAs and lncRNAs in thyroid carcinogenesis were recently investigated (Brown et al., 2014, Sedaghati and Kebebew, 2019, Colamaio et al., 2015).

The aim of this study was the identification and characterization of molecular processes in the early stages of the carcinogenic processes in the thyroid. For this purpose, we used a mouse model and performed comprehensive histological analyses of thyroids from a cohort of mice that received low-dose gamma-irradiation early in life. Subsequently, laser capture microdissection (LCM) enabled transcriptomic profiling of histologically normal and aberrant tissue areas, in order to gain further insight in early events of genetic and molecular deregulation that may drive the early phases of thyroid malignancies.

MATERIAL and METHODS

Workflow

The entire workflow of this study is visualized in Figure 1.

Thyroid tissues

Mouse thyroids were obtained from the INSTRA lifetime study and details on mice are presented in Dalke et al. (Dalke et al., 2018). 164 mice were whole body irradiated at the age of 10 weeks with different doses of 0.063 Gy, 0.125 Gy and 0.5 Gy. 82 mice exposed to 0 Gy served as control group (sham irradiation). Animals were sacrificed at pre-determined time points (6 months, 12 months, 18 months, 24 months) and

thyroids were collected. Details of all mice and histopathologically examined samples are shown in SI Table 1, and samples analyzed by RNAseq are shown in SI Table 2. Approximately 50% of the mice included in the study harbor a heterozygous mutation of the ERCC2 gene. This mutation was investigated for its potential to promote eye lens cataracts after exposure to ionizing radiation in a previous study, while explicitly no association of thyroid aberrations and ERCC2 gene mutation was reported. The study also provides a detailed description of the genomic background of these mice (Dalke et al., 2018).

Tissue processing and comprehensive histological examination

Tissues were snap-frozen in liquid nitrogen upon resection and embedded in a Cryo Gel (Leica Surgipath Cryogel) before transversal sectioning. A total number of 246 thyroids were exhaustively processed into 30 µm and 12 µm tissue sections. While the series of 30 µm sections were kept for potential laser capture microdissection (LCM), the 12 µm sections were stained with hematoxylin and eosin (HE) for histopathological evaluation. Dependent on the size, 10 to 20 thyroid sections were analyzed histopathologically. The sections were independently examined by to pathologists (A.W. and A.B.). All thyroid samples were investigated and classified based on the WHO criteria for the evaluation of murine thyroid tumors and according to the international classification of rodent tumors (Jokinen and Botts, 1994, DeLellis RA, 2004, Capen, 2001). Normal thyroid tissues were classified by variable-sized follicles covered by monolayers of flattened epithelial cells. Further, hyperplastic thyroid tissues were diagnosed by the occurrence of small follicles showing scant colloid and tall epithelial cells adjacent to normal follicles. In contrast, neoplastic thyroid lesions

193 such as adenomas were identified by the presence of demarcated histologic areas
194 with a distinct follicular and/or papillary architecture. To differentiate those neoplastic
195 lesions from carcinomas, the invasion of the surrounding glandular parenchyma or
196 stroma was evaluated. Due to the absence of such invasive areas, there was no
197 indication for carcinomas of the papillary or follicular subtype in any of the neoplastic
198 cases. Furthermore, the presence of immune cells was quantitatively assessed in the
199 evaluated HE slides. Immune cell infiltration was expressed as the number of immune
200 cells per section area (cells/mm^2) and was determined in 2-3 sections per case. After
201 histological analysis, two groups of tissue samples were defined: the first group
202 comprised proliferative lesions from the irradiated mice, and the second group
203 contained morphologically normal tissue taken from the same animal, respectively. A
204 third group of normal thyroid tissues from sex- and age-matched non-irradiated mice
205 was added. For molecular investigation 30 µm thick sections were prepared for LCM.
206 LCM was carried out utilizing a PALM MicroBeam device (Zeiss, Germany), which
207 allows the dissection and collection of targeted tissue formations or groups of cells
208 after microscopic identification, according to the manufacturers protocol and as
209 previously described (Morrogh et al., 2007).
210 The histological findings in irradiated and non-irradiated mice were statistically
211 analyzed by Fisher's exact test. Immune cell scores were compared between the three
212 groups by the analysis of variance (ANOVA) and pair-wise compared by post-hoc Tukey
213 test. Statistical significance was considered at $p < 0.05$.
214

215 **RNA isolation and RNAseq 3´library preparation**

The RNA extraction from the laser capture microdissected cells was performed with the RNeasy Micro Kit (Quiagen), according to the manufacturer's protocol. RNA quality was evaluated using a Bioanalyzer 2100 Systems (Agilent Technologies, Inc., USA) with Agilent RNA 6000 Pico Kit (#5067-1513, Agilent Technologies, Inc., USA). RNA integrity was assessed by calculation of the percentage of fragments >200 nucleotides (DV200, SI Table 3). Sequencing libraries were generated using 50 ng of total RNA and the QuantSeq 3′ mRNA-Seq Library Prep Kit FWD for Illumina (SKU: 015.96, Lexogen GmbH, Austria). Library amplification PCR cycles were determined using PCR Add-on Kit for Illumina (SKU: 020.96, Lexogen GmbH, Austria) and the individual libraries were amplified with 17 PCR cycles. Quality and quantity of the libraries were evaluated using the Quanti-iT PicoGreen dsDNA Assay Kit (P7589, Invitrogen, USA) and the Bioanalyzer High Sensitivity DNA Analysis Kit (#5067-4626, Agilent Technologies, Inc., USA). 150 bp paired-end sequencing was performed on an Illumina HiSeq4000 platform (Illumina, Inc., USA). Lexogen QuantSeq 3′ library preparation was chosen for RNAseq analysis because it has the capability to generate high quality gene expression data from low amounts (down to 10 pg) and/or compromised quality of total RNA. Both properties were expected from the small LCM-specimens used for RNAseq analysis.

RNAseq data analysis, differential expression analysis, Gene Set Enrichment Analysis (GSEA) and Pathway RespOnsive GENes analysis (PROGENy)

Raw data as well as preprocessed RNAseq data are available from Gene Expression Omnibus (GEO accession number: GSE162795). Gene expression quantification was carried out by alignment of RNAseq reads to the mouse reference genome (Ensembl

GRCm38 version 94) using the STAR aligner, followed by count quantification using the featureCounts of the Rsubreads R package (Dobin et al., 2013, Liao et al., 2014). Differential gene expression analysis was performed using methods implemented in the *DESeq2* R package (Love et al., 2014). Principal component analysis was carried out on variance stabilized read counts. Differential expression between proliferative lesions and corresponding normal tissue samples (PL vs. NT) was performed with a paired design, while normal tissue vs. normal control tissue and proliferative lesions vs. normal control tissue (NT vs. NCT, PL vs. NCT), were analyzed in group comparisons controlled for sex and age. Genes with an absolute log2-fold change > 0.5 and an adjusted p-value < 0.1 were considered differentially expressed. The log2-fold change (log2-FC) and adjusted p-value thresholds were used solely to visualize the results of the differential expression analysis, but no functional interpretations were based on them. *Gene Set Enrichment Analysis* (GSEA) was conducted in a pre-ranked mode using the log2-FC values obtained from *DESeq2* (log-fold-change-shrinkage) for the ranking of the gene list using the *fgsea* R package (Sergushichev, 2016, Powers et al., 2018). The Hallmark gene sets (n=50), downloaded from Molecular Signature Database (http://software.broadinstitute.org/gsea/msigdb/index.jsp), plus additional thyroid pathogenesis-related or cancer-associated gene sets taken from the KEGG (n=41) and Reactome (n=23) gene set collections were used for enrichment testing (SI Table 4). PROGENy analysis was carried out in order to test for a deregulation in eleven cancer relevant signal transduction pathways using transcriptomics data. In comparison to conventional pathway analysis methods (e.g. GSEA), PROGENy infers pathway activity based on consensus gene signatures obtained from perturbation

experiments on protein level and constitutes the footprint on gene expression (Schubert, 2017).

qRT-PCR validation of RNAseq quantification

In addition to the technical quality control of the RNAseq data using FastQC, their validity was investigated by comparing the expression of eight randomly selected genes determined by RNAseq with that determined by qRT-PCR in all 27 samples. Four of the selected genes (CD36, HSP90AA1, IL1B, SERPINE1) were differentially expressed in one of the three comparisons carried out and four (ALAS1, LRP1, PLAU, THBS1) that did not show differential expression. Total RNA extracted from mouse tissue samples was processed and analyzed by qRT-PCR as described before (Krombach et al., 2019). Relative expression values were determined as delta CT-values to a reference gene matrix of 18S rRNA and beta-actin with efficiency correction via three different cDNA dilutions for each sample. Pearson correlation between RNAseq and qRT-PCR determined gene expression was used as a measure of concordance.

Clustering of samples using a literature-derived gene set

A literature-derived gene set consisting of 85 thyroid carcinogenesis- and thyroid cancer-associated genes, was utilized for hierarchical clustering of samples using correlation as distance measure (linkage “complete”) followed by visualization as heatmap including the cluster dendrogram using the *pheatmap* R package. The considered publications reported the genes to be associated with thyroid carcinogenesis and cancer and in greater detail with proliferation, metabolic

deregulation, and immune signaling (Rusinek et al., 2011, Vella and Malaguarnera, 2018, Xing, 2013, Giuliani et al., 2018).

A subset of these genes was also present in the gene expression data set generated on the normal tissue and PTC tissue from the Ukranian-American cohort (UkrAM) of human individuals who were exposed to ionizing radiation as a consequence of the Chernobyl reactor accident (Abend et al., 2013). Their expression levels were compared to the expression data from the three histological groups generated in this study.

RESULTS

Histological analysis reveals radiation-associated lesions

The histological analysis revealed nine mice with proliferative lesions in the thyroid (PL) out of 246 animals in total. PLs were exclusively present in the irradiated group while seven PLs were observed in the 24 months group (p=0.09) and two in the 18 months group (p=1). No significant difference with regard to the sex of animals was detected (male p=0.55; female p=0.18). Fisher´s exact test for the frequency of PLs in the irradiated and non-irradiated group (9/164 exposed, 0/82 non-exposed) indicated a significant association between PL-occurrence and radiation exposure (p=0.03). Three out of nine alterations met the diagnostic criteria of an adenoma according to Capen's Classification (Capen, 2001). The remaining six cases were classified as follicular hyperplasia. Eventually, all nine lesions showed predominantly a papillary pattern, which is characterized by branching infoldings covered by a single-layered epithelium. While follicular hyperplasia is not well demarcated, adenomas often have

a more complex architecture accompanied by encapsulation (Capen, 2001). Since any signs of invasion of surrounding tissue or blood vessels were absent, none of the neoplastic lesions were classified as carcinoma. Immune cells (lymphocytes, neutrophils, plasma cells, and macrophages) were investigated, both, in irradiated and non-irradiated tissues and cells were counted to quantify the extent of infiltration. The highest density of immune cells was detected in proliferative tissue, followed by normal irradiated tissue and non-irradiated normal tissue. Microscopic images visualizing the location of the lesions within the thyroid glands, exemplary high-resolution images of the examined tissues, and the observed immune cell densities within the different tissues are provided in SI Figure 1. Statistically significant differences in immune cell densities (infiltration) were identified by ANOVA ($p<0.01$) and post-hoc Tukey's test between proliferative and normal irradiated tissue (PL compared to NT, $p=0.01$) and between proliferative and non-irradiated normal tissue (PL compared to NCT, $p=0.001$). No significant difference between irradiated normal tissue and non-irradiated normal tissue was observed (NT compared to NCT, $p=0.23$, SI Figure 2). Sample information and histological classifications are summarized in SI Table 1 and SI Table 2.

qRT-PCR validation of RNAseq quantification

Pearson correlation coefficients ranged from 0.53 to 0.91 for seven out of the eight genes investigated, only the HSP90AA1 gene exhibited a correlation coefficient of 0.21 (SI Table 5). These finding validate the 3′ RNAseq data, since only one gene detected with primers located near the 5′ end indicated low correlation.

Transcriptomic analysis points at deregulated pathways in normal tissue and proliferative lesions

Principal component analysis (PCA) of the RNAseq transcriptome data set exhibited grouping of the samples according to their histological classification, separating proliferative lesion samples (PL) very well from the corresponding normal tissue samples (NT) and normal control tissue samples (NCT). The separation of NT and NCT was less pronounced (Figure 1, C). Dimensionality reduction by multi-dimensional-scaling (MDS) and PCA using the top-500 variant genes in the data set are provided in SI Figure 3C/D, PC loadings are provided in SI Table 6 and SI Table 7. PROGENy analysis revealed an activated EGFR, MAPK and TNFa signal transduction in NT compared to NCT. The most prominent finding in PL compared to NT was a downregulated p53 signaling, while PL compared to NCT showed elevated proliferation-associated signaling (MAPK, PI3K, EGFR) and downregulated p53 signaling (Figure 2A, SI Table 8). With respect to log2-FC and false discovery rate (FDR), differential gene expression was least pronounced in NT compared to NCT (128 genes), followed by PL compared to NT (1355 genes), and PL compared to NCT (2379 genes), respectively (Figure 2C, SI Table 9). Common and specific genes for the three comparisons are visualized in SI Figure 4. Gene set enrichment analysis (GSEA) is visualized in Figure 2D. All gene sets with an FDR < 0.1 in at least one out of the three comparisons were included into the plot. Mainly, activated immune signaling and a downregulated metabolic signaling in NT compared to NCT and activated proliferation-associated signaling and downregulated metabolic signaling in PT compared to NT was found (Figure 2D) while PL compared to NCT showed increased proliferation-associated signaling.

Hierarchical clustering of histological groups based on literature-derived gene set

Hierarchical clustering analysis, based on the expression of the literature-derived and thyroid cancer-associated gene set (85 genes) resulted in three main clusters, separating the three histologically defined groups (SI Figure 3A). Additionally, the cluster affiliations were visualized in the PCA and MDS plots in Figure 3B-D. 31 out of the 85 genes were differentially expressed (SI Table 9). Mouse expression data were compared to human expression data using the microarray expression data set of thyroid cancers developed in the UkrAm cohort (Tronko et al., 2006). The expression levels of 26 out of the 31 differentially expressed genes were also present in the data set on human PTC. Differential expression of 14 out of these 26 genes in the human data, indicates their relevance in thyroid cancer/carcinogenesis in human and mouse tissue and the relevance of the studied tissues as a model for thyroid carcinogenesis (SI Figure 5 and SI Figure 6).

DISCUSSION

This study aimed to elucidate early stages of thyroid tumorigenesis by investigating histological and molecular changes in mouse thyroids derived from mice after one-time exposure to ionizing radiation (Dalke et al., 2018). Besides the finding presented in this study, Dalke et al. reported an association of one-time exposure to ionizing radiation with increased body weight, reduced survival rates and a dose-dependent association with several other tumor types and eye lens opacity (Dalke et al., 2018). Mouse models are a valid tool to study the molecular mechanisms underlying thyroid tumorigenesis since it has been shown that large biological and histological similarities

between human thyroid and mouse thyroid exist (Perlman, 2016). However, the definitions of pre-neoplastic and neoplastic lesions diverge (Baloch and LiVolsi, 2018, DeLellis RA, 2004, Capen, 2001, Boorman G A, 1995). The different histological phenotypes and their histopathological classifications make a comparative diagnosis between the different cancer entities in mice and humans challenging. In this study, tissue samples were examined on the basis of Capen's International Classification of Rodent Tumors (Capen, 2001), which does not distinguish between the different histological entities. Therefore, a comparative investigation of a specific cancer entity was not possible. Instead, we focused on early molecular processes of thyroid tumorigenesis that occurred in histologically normal and aberrant mouse thyroid tissues. While tumor initiation, promotion and progression in murine thyroids starts with proliferative lesions (e.g. hyperplasia), followed by follicular adenoma, which subsequently progress to follicular thyroid carcinoma, in humans it is more complex and is reflected by different thyroid carcinoma subtypes (DeLellis RA, 2004, Capen, 2001, Boorman G A, 1995).

Comprehensive histological examination of 164 exposed and 82 non-exposed thyroids revealed neoplastic alterations exclusively in exposed mice, which is in line with multiple previous studies reporting ionizing radiation as one of the major risk factors for the development of thyroid carcinoma (Mullenders et al., 2009, Cardis et al., 2005, Williams, 2008, Zablotska et al., 2008, Furukawa et al., 2013, La Vecchia et al., 2015, Ron, 2007). While adenomas were identified within the exposed group, we did not observe any carcinoma in our study. This might be due to the limited life span of a mouse and the fact that the experiment was terminated at 24 months, which might not allow full progression of the carcinogenic process. These observations might

406 reflect the widely acknowledged stepwise model of progression to cancer, in which
407 the accumulation of mutations or other events leads to successive clonal expansion
408 and aberrant phenotypes (Martincorena and Campbell, 2015, Laconi et al., 2020).
409 Barrett's esophagus is one prominent example of a precursor lesion on the road to
410 malignancy, where a metaplasia-dysplasia-carcinoma sequence seems to be proven
411 (Weaver et al., 2014). Although, we did not perform mutation typing, our findings
412 support the stepwise model concept at the transcriptome and functional levels and
413 provide insights for the poorly studied area of precancerous thyroid lesions.
414 It is generally accepted that inflammation is linked to cancer development (Mantovani
415 et al., 2008). In thyroid cancer, the inflammatory tumor microenvironment, containing
416 immune cells and mediators like chemokines, plays a central role in the carcinogenesis
417 and is among the hallmarks of cancer (Yapa et al., 2017, Hanahan and Weinberg,
418 2011). Tumor microenvironment as mutation promoter is discussed as potential driver
419 of field cancerization of various cancer entities (Curtius et al., 2018). Although no
420 acute inflammation was observed in the examined tissues, the number of immune
421 cells present in the different histological groups steadily increased from normal
422 control tissue (NCT), to normal tissue (NT), to proliferative lesions (PL) (SI Figure2).
423 The elevated immune cell numbers in NT and PL tissues potentially indicate
424 deregulated chemokine expression that triggers physiologic changes and immune
425 responses by the recruitment of specific immune cell populations to the tissue sites.
426 Neoplastic thyroid cells have the ability to alter the chemokine system for their own
427 benefit by influencing immune cell recruitment into the tumor microenvironment,
428 thereby affecting multiple aspects of thyroid cancer progression (Yapa et al., 2017).
429 These findings integrate well with elevated immune signaling in NT and PL tissues as

shown by RNAseq analysis (GSEA and PROGENy) and potentially explain the increased numbers of immune cells in these tissues (Figure 2, SI Figure 2).

In order to analyze the histologically defined tissue regions on molecular level, we established a technically challenging workflow: Firstly, we collected the cells forming the tissue regions of interest (PL, NT, NCT) from the tissue sections by LCM prior to extraction of total RNA from these comparably small numbers of cells, followed by high-quality RNA-sequencing library generation and RNA sequencing. Transcriptomic data were used to delineate molecular changes in histologically normal thyroid tissue (NT) and adjacent proliferative lesions that underwent a tumorigenic process (PL). Normal control tissues of non-irradiated mice (NCT) without any histological aberrations in the entire thyroid were used as a reference. Although, the differential expression analysis between NT and NCT showed the lowest level of transcriptomic deregulation within the three conducted differential expression analysis (log2-FC, adjusted-p-value, Volcano plots, Figure 2B), the deregulation was significantly functionally associated with tumorigenesis by PROGENy and GSEA. Despite the different concepts of functional association of transcriptomic deregulation in PROGENy and GSEA, the derived results integrate well and are biologically plausible in the context of the study.

The PROGENy results fit the concept of a progression model while the level of deregulation accumulates from healthy, histologically normal tissue (NCT) to histologically normal tissue with a deregulated molecular phenotype, that progresses further into tissue with histological abnormalities (PL). As an example (Figure 2A), the p53-signaling was weakly upregulated in NT compared to NCT and strongly downregulated in PL compared to NT, resulting in less pronounced downregulation in

PL compared to NCT. Contrarily, MAPK-signaling was highly upregulated in NT compared to NCT and PL compared to NCT, but did not show a difference in PL compared to NT. These observations allow the interpretation that the apoptotic processes mediated by p53 prevented the NT tissues that already showed an activated MAPK response, from excessive proliferation (which would be histologically visible), while the activated MAPK response potentially led to excessive proliferation in PL, were the p53 associated apoptosis is downregulated and cannot "counter-act" the MAPK signaling. Observations for the NF-κB response are qualitatively identical and integrate well with this interpretation (Figure 2A). Additionally, Pi3K signaling is activated in NT and PL compared to NCT. PI3K deregulation was previously described in association with follicular thyroid carcinoma and with anaplastic thyroid carcinoma (ATC) in conjunction with a MAPK cascade deregulation (Xing, 2013).

The most prominent GSEA findings (Figure 2,D) in the comparison between NT and NCT are the elevated immune response signaling, comprised of gene sets representing allograft rejection, interferon alpha/gamma response, inflammatory response and TNFa via NF-κB signaling and confirm the PROGENY results that show an activated TNFa and NF-κB response in NT compared to NCT.

The NF-κB signaling pathway is one potential link between cancer and inflammation in thyroid carcinogenesis and a proven common mechanism to activate cell survival, proliferation and differentiation, contributing to tumor progression (Karin, 2009, Li et al., 2013). It is interesting to note that, NF-κB signaling might either promote tumor growth by activating cell proliferation and angiogenesis or acts anti-tumorigenically by triggering an immune response and the attraction of immune cells (Pires et al., 2018, Pacifico et al., 2004). This could further explain the elevated proliferation-

associated signaling on molecular level, without the presence of histological aberrations in NT tissues. Negatively enriched gene sets in the comparison of NT with NCT were exclusively associated with metabolic processes (Figure 2, D). These findings integrate well with the recently reported emerging role of the insulin receptor in the context of carcinogenesis of several malignant diseases including thyroid cancer (Vella and Malaguarnera, 2018).

Consistently, proliferative lesions (PL) compared to the adjacent normal tissues (NT) showed strongly activated proliferation-associated processes, along with increased signals for immune-associated gene sets, while the immune-associated deregulation was not as strong as in NT compared to NCT. From these findings, we concluded that molecular deregulations leading to an activation of the immunologic processes, such as metabolic processes, are already present in histologically normal tissues (NT). Metabolic processes in PL-NCT and NT-NCT show similar regulation patterns, including the peroxisome- and lysosome-associated gene that suggest differences in the metabolic transport processes in NT and PL tissues.

Additionally, KRAS signaling was deregulated in all three comparisons, while the signal appears fundamentally different in PL-NT and PL-NCT compared NT-NCT (Figure 2,D), potentially indicating a mutation in this pathway. KRAS, along with other RAS mutations, was described in association with deregulated cell proliferation in multiple cancer entities (Xing, 2016).

Confirmatory studies on protein level and data on the BRAF V600E mutation status, genomic rearrangements, such as RET/PTC rearrangements and PAX8-PPARG fusions, which are frequently described in thyroid carcinoma would be desirable to further

support the conclusions drawn from this study. However, this was not feasible due to the limited amounts of tissue derived from the small LCM-specimen.

While multiple studies discuss the effect of specific genes on a single process of thyroid carcinogenesis, we aimed at an integrated analysis by applying a hierarchical clustering approach on the transcriptomic data. Using 85 thyroid carcinogenesis and thyroid cancer-associated genes derived from the literature (SI Table 10, functional grouping and citations), separation into three defined histological groups was achieved. This suggests that carcinogenic processes are already ongoing within the proliferative lesions of this study thus representing early stages of thyroid tumorigenesis. The expression levels in the three histologic groups of multiple thyroid carcinogenesis- and cancer-associated genes indicate that the analyzed tissues represent sequential stages of molecular and histologic transformation in thyroid tumorigenesis. Increasing expressions from NCT, via NT, to PL for the thyroid tumor-promoting genes TSHR, IDH1, NFKB1, HIF1AN, STAT3, TPO, TRP53, TMEM173 (STING), IGF1, MAPK10 and decreasing expressions for tumor-suppressing genes such as SLC5A8, TIMP3, ITIH5, PCSK2 were observed (Figure 2B, SI Figure 5, SI Table 10). This further underlines that the PL tissues might represent early stages during thyroid tumorigenesis and that histologically normal tissues (NT) already show molecular deregulations pointing to the development of thyroid cancer.

Additionally, 26 out of the 31 differentially expressed genes in the 85-gene set that were present in the human UkrAm gene expression data set showed similar regulation patterns and significant differential expression between normal tissue and tumor tissue (PTC) samples compared to the expression data generated within this study (SI Figure 5 and 6). This indicates that these genes that are known to be deregulated

525 during the early phases of the carcinogenic process remain to be deregulated in
526 human PTC and confirm the herein studied tissues as a relevant model for the early
527 phases of thyroid tumorigenesis.
528 In NT, our study design, which was also determined by limited availability of
529 biomaterial, does not allow for a clear discrimination between potential radiation
530 effects and early processes towards proliferative thyroid lesions at the transcriptome
531 level. Nevertheless, regardless of the trigger we were able to detect functionally
532 relevant deregulation that is conclusive with respect to the affected molecular
533 processes and integrates well with findings within the present and previous studies
534 on thyroid carcinogenesis and early-stage processes of several other cancer entities.
535

536 **CONCLUSION**

537

538 In conclusion, we hypothesize that the histologically normal tissues (NT), which
539 contain no macroscopically detectable abnormalities, represent a very early stage in
540 thyroid carcinogenesis and will further progress to thyroid hyperplasia, followed by
541 thyroid adenoma and potentially by thyroid carcinoma. While NT tissues exhibit
542 histologically normal structures, the molecular footprint compared to normal control
543 tissues (NCT) already indicates an initiation of carcinogenic processes. These findings
544 integrate well with the proposed multi-step model and the fetal cell carcinogenesis
545 model as discussed in Zane et al. (Zane et al., 2016). Potential clinical implication might
546 be a refined thyroid cancer diagnosis, which is currently carried out by fine needle
547 biopsy followed by cytologic classification. Further investigation of thyroid tissues with

normal histology and deregulated molecular levels are necessary in order to develop a molecular signature or marker for implementation in routine clinical diagnostics.

Declaration of interest, Funding and Acknowledgements

Funding:

The INSTRA project is funded by the Bundesministerium für Bildung und Forschung (BMBF) [grant number 02NUK045A], while no influence or suggestions were made with respect to the collection, analysis and interpretation of data, the writing of the report and the decision to submit the article for publication.

Author Disclosure Statement:

No conflicts of interests or competing financial interests exist.

Ethical standards:

All applicable international, national and/or institutional guidelines for the care and use of animals were followed. In particular, the study was approved by the government of Upper Bavaria (Az. 55.2-1-54-2532-161-12).

Acknowledgements:

We thank Laura Dajka, Claire Innerlohinger, Aaron Selmeier, Isabella Zagorski and Steffen Heuer for their excellent technical support.

572 Public availability of RNAseq data:

573 GEO accession number GSE162795

574

575 **LITERATURE**

576

577 ABEND, M., PFEIFFER, R. M., RUF, C., HATCH, M., BOGDANOVA, T. I., TRONKO, M. D.,
578 HARTMANN, J., MEINEKE, V., MABUCHI, K. & BRENNER, A. V. 2013. Iodine-131 dose-
579 dependent gene expression: alterations in both normal and tumour thyroid tissues
580 of post-Chernobyl thyroid cancers. *Br J Cancer,* 109**,** 2286-94.
581 BALOCH, Z. W. & LIVOLSI, V. A. 2018. Special types of thyroid carcinoma. *Histopathology,* 72**,**
582 40-52.
583 BOORMAN G A, S. R. C., HAILEY J R 1995. Preneoplastic and Neoplastic Lesions of the Rat and
584 Mouse Thyroid. *In:* BANNASCH P, G. W. (ed.) *Pathology of Neoplasia and*
585 *Preneoplasia in Rodents.* Stuttgart New York: Schattauer.
586 BROWN, T. C., JUHLIN, C. C., HEALY, J. M., PRASAD, M. L., KORAH, R. & CARLING, T. 2014.
587 Frequent silencing of RASSF1A via promoter methylation in follicular thyroid
588 hyperplasia: a potential early epigenetic susceptibility event in thyroid
589 carcinogenesis. *JAMA Surg,* 149**,** 1146-52.
590 CAHOON, E. K., NADYROV, E. A., POLYANSKAYA, O. N., YAUSEYENKA, V. V., VEYALKIN, I. V.,
591 YEUDACHKOVA, T. I., MASKVICHEVA, T. I., MINENKO, V. F., LIU, W., DROZDOVITCH,
592 V. et al.v 2017. Risk of Thyroid Nodules in Residents of Belarus Exposed to Chernobyl
593 Fallout as Children and Adolescents. *J Clin Endocrinol Metab,* 102**,** 2207-2217.
594 CAPEN, C. 2001. Endocrine System-Thyroid Gland. *In:* MOHR, U. (ed.) *International*
595 *Classification of Rodent Tumours. The Mouse.* Springer.
596 CARDIS, E., KESMINIENE, A., IVANOV, V., MALAKHOVA, I., SHIBATA, Y., KHROUCH, V.,
597 DROZDOVITCH, V., MACEIKA, E., ZVONOVA, I., VLASSOV, O. et al. 2005. Risk of
598 thyroid cancer after exposure to 131I in childhood. *J Natl Cancer Inst,* 97**,** 724-32.
599 COLAMAIO, M., PUCA, F., RAGOZZINO, E., GEMEI, M., DECAUSSIN-PETRUCCI, M., AIELLO, C.,
600 BASTOS, A. U., FEDERICO, A., CHIAPPETTA, G., DEL VECCHIO, L. et al. 2015. miR-142-
601 3p down-regulation contributes to thyroid follicular tumorigenesis by targeting
602 ASH1L and MLL1. *J Clin Endocrinol Metab,* 100**,** E59-69.
603 CURTIUS, K., WRIGHT, N. A. & GRAHAM, T. A. 2018. An evolutionary perspective on field
604 cancerization. *Nat Rev Cancer,* 18**,** 19-32.
605 DALKE, C., NEFF, F., BAINS, S. K., BRIGHT, S., LORD, D., REITMEIR, P., ROSSLER, U., SAMAGA,
606 D., UNGER, K., BRASELMANN, H. et al., J. 2018. Lifetime study in mice after acute
607 low-dose ionizing radiation: a multifactorial study with special focus on cataract risk.
608 *Radiat Environ Biophys,* 57**,** 99-113.
609 DELELLIS RA, W. E. 2004. Tumors of the Thyroid and Parathyroid. *In:* DELELLIS RA, L. R. H. P.,
610 ENG C (ed.) *World Health Organization (WHO) Classification of Tumors-Pathology*
611 *and Genetics of Tumours of Endocrine Organs.* Lyon: IARC Press.
612 DOBIN, A., DAVIS, C. A., SCHLESINGER, F., DRENKOW, J., ZALESKI, C., JHA, S., BATUT, P.,
613 CHAISSON, M. & GINGERAS, T. R. 2013. STAR: ultrafast universal RNA-seq aligner.
614 *Bioinformatics,* 29**,** 15-21.
615 EFANOV, A. A., BRENNER, A. V., BOGDANOVA, T. I., KELLY, L. M., LIU, P., LITTLE, M. P., WALD,
616 A. I., HATCH, M., ZURNADZY, L. Y., NIKIFOROVA, M. N. et al. 2018. Investigation of

the Relationship Between Radiation Dose and Gene Mutations and Fusions in Post-Chernobyl Thyroid Cancer. *J Natl Cancer Inst,* 110**,** 371-378.

FURUKAWA, K., PRESTON, D., FUNAMOTO, S., YONEHARA, S., ITO, M., TOKUOKA, S., SUGIYAMA, H., SODA, M., OZASA, K. & MABUCHI, K. 2013. Long-term trend of thyroid cancer risk among Japanese atomic-bomb survivors: 60 years after exposure. *Int J Cancer,* 132**,** 1222-6.

GIULIANI, C., BUCCI, I. & NAPOLITANO, G. 2018. The Role of the Transcription Factor Nuclear Factor-kappa B in Thyroid Autoimmunity and Cancer. *Front Endocrinol (Lausanne),* 9**,** 471.

HANAHAN, D. & WEINBERG, R. A. 2011. Hallmarks of cancer: the next generation. *Cell,* 144**,** 646-74.

JOKINEN, M. P. & BOTTS, S. 1994. Tumours of the thyroid gland. *IARC Sci Publ***,** 565-94.

JUNG, S. H., KIM, M. S., JUNG, C. K., PARK, H. C., KIM, S. Y., LIU, J., BAE, J. S., LEE, S. H., KIM, T. M., LEE et al. 2016. Mutational burdens and evolutionary ages of thyroid follicular adenoma are comparable to those of follicular carcinoma. *Oncotarget,* 7**,** 69638-69648.

KARIN, M. 2009. NF-kappaB as a critical link between inflammation and cancer. *Cold Spring Harb Perspect Biol,* 1**,** a000141.

KAZAKOV, V. S., DEMIDCHIK, E. P. & ASTAKHOVA, L. N. 1992. Thyroid cancer after Chernobyl. *Nature,* 359**,** 21.

KONDO, T., EZZAT, S. & ASA, S. L. 2006. Pathogenetic mechanisms in thyroid follicular-cell neoplasia. *Nat Rev Cancer,* 6**,** 292-306.

KROMBACH, J., HENNEL, R., BRIX, N., ORTH, M., SCHOETZ, U., ERNST, A., SCHUSTER, J., ZUCHTRIEGEL, G., REICHEL, C. A., BIERSCHENK et al. 2019. Priming anti-tumor immunity by radiotherapy: Dying tumor cell-derived DAMPs trigger endothelial cell activation and recruitment of myeloid cells. *Oncoimmunology,* 8**,** e1523097.

LA VECCHIA, C., MALVEZZI, M., BOSETTI, C., GARAVELLO, W., BERTUCCIO, P., LEVI, F. & NEGRI, E. 2015. Thyroid cancer mortality and incidence: A global overview. *Int J Cancer,* 136**,** 2187-95.

LACONI, E., MARONGIU, F. & DEGREGORI, J. 2020. Cancer as a disease of old age: changing mutational and microenvironmental landscapes. *Br J Cancer,* 122**,** 943-952.

LI, X., ABDEL-MAGEED, A. B., MONDAL, D. & KANDIL, E. 2013. The nuclear factor kappa-B signaling pathway as a therapeutic target against thyroid cancers. *Thyroid,* 23**,** 209-18.

LIAO, Y., SMYTH, G. K. & SHI, W. 2014. featureCounts: an efficient general purpose program for assigning sequence reads to genomic features. *Bioinformatics,* 30**,** 923-30.

LOVE, M. I., HUBER, W. & ANDERS, S. 2014. Moderated estimation of fold change and dispersion for RNA-seq data with DESeq2. *Genome Biol,* 15**,** 550.

MANTOVANI, A., ALLAVENA, P., SICA, A. & BALKWILL, F. 2008. Cancer-related inflammation. *Nature,* 454**,** 436-44.

MARTINCORENA, I. & CAMPBELL, P. J. 2015. Somatic mutation in cancer and normal cells. *Science,* 349**,** 1483-9.

MORROGH, M., OLVERA, N., BOGOMOLNIY, F., BORGEN, P. I. & KING, T. A. 2007. Tissue preparation for laser capture microdissection and RNA extraction from fresh frozen breast tissue. *Biotechniques,* 43**,** 41-2, 44, 46 passim.

MULLENDERS, L., ATKINSON, M., PARETZKE, H., SABATIER, L. & BOUFFLER, S. 2009. Assessing cancer risks of low-dose radiation. *Nat Rev Cancer,* 9**,** 596-604.

NIKIFOROV, Y. E. 2006. Radiation-induced thyroid cancer: what we have learned from chernobyl. *Endocr Pathol,* 17**,** 307-17.

NIKIFOROV, Y. E. & NIKIFOROVA, M. N. 2011. Molecular genetics and diagnosis of thyroid cancer. *Nat Rev Endocrinol,* 7**,** 569-80.

NIKIFOROVA, M. N. & NIKIFOROV, Y. E. 2008. Molecular genetics of thyroid cancer: implications for diagnosis, treatment and prognosis. *Expert Rev Mol Diagn,* 8**,** 83-95.

PACIFICO, F., MAURO, C., BARONE, C., CRESCENZI, E., MELLONE, S., MONACO, M., CHIAPPETTA, G., TERRAZZANO, G., LIGUORO, D., VITO, P. et al. 2004. Oncogenic and anti-apoptotic activity of NF-kappa B in human thyroid carcinomas. *J Biol Chem,* 279**,** 54610-9.

PERLMAN, R. L. 2016. Mouse models of human disease: An evolutionary perspective. *Evol Med Public Health,* 2016**,** 170-6.

PIRES, B. R. B., SILVA, R., FERREIRA, G. M. & ABDELHAY, E. 2018. NF-kappaB: Two Sides of the Same Coin. *Genes (Basel),* 9.

POWERS, R. K., GOODSPEED, A., PIELKE-LOMBARDO, H., TAN, A. C. & COSTELLO, J. C. 2018. GSEA-InContext: identifying novel and common patterns in expression experiments. *Bioinformatics,* 34**,** i555-i564.

RON, E. 2007. Thyroid cancer incidence among people living in areas contaminated by radiation from the Chernobyl accident. *Health Phys,* 93**,** 502-11.

RON, E., LUBIN, J. H., SHORE, R. E., MABUCHI, K., MODAN, B., POTTERN, L. M., SCHNEIDER, A. B., TUCKER, M. A. & BOICE, J. D., JR. 1995. Thyroid cancer after exposure to external radiation: a pooled analysis of seven studies. *Radiat Res,* 141**,** 259-77.

RUSINEK, D., SZPAK-ULCZOK, S. & JARZAB, B. 2011. Gene expression profile of human thyroid cancer in relation to its mutational status. *J Mol Endocrinol,* 47**,** R91-103.

SCHUBERT, M. 2017. Perturbation-response genes reveal signaling footprints in cancer gene expression. *Nature Communicationsvolume,* 9.

SEDAGHATI, M. & KEBEBEW, E. 2019. Long noncoding RNAs in thyroid cancer. *Curr Opin Endocrinol Diabetes Obes,* 26**,** 275-281.

SERGUSHICHEV, A. 2016. An algorithm for fast preranked gene set enrichment analysis using cumulative statistic calculation. *bioRxiv*.

SPONZIELLO, M., LAVARONE, E., PEGOLO, E., DI LORETO, C., PUPPIN, C., RUSSO, M. A., BRUNO, R., FILETTI, S., DURANTE, C., RUSSO, D. et al, 2013. Molecular differences between human thyroid follicular adenoma and carcinoma revealed by analysis of a murine model of thyroid cancer. *Endocrinology,* 154**,** 3043-53.

TRONKO, M. D., HOWE, G. R., BOGDANOVA, T. I., BOUVILLE, A. C., EPSTEIN, O. V., BRILL, A. B., LIKHTAREV, I. A., FINK, D. J., MARKOV, V. V., GREENEBAUM, E., OLIJNYK, V. A. et al. 2006. A cohort study of thyroid cancer and other thyroid diseases after the chornobyl accident: thyroid cancer in Ukraine detected during first screening. *J Natl Cancer Inst,* 98**,** 897-903.

VELLA, V. & MALAGUARNERA, R. 2018. The Emerging Role of Insulin Receptor Isoforms in Thyroid Cancer: Clinical Implications and New Perspectives. *Int J Mol Sci,* 19.

VOGELSTEIN, B. & KINZLER, K. W. 1993. The multistep nature of cancer. *Trends Genet,* 9**,** 138-41.

WEAVER, J. M. J., ROSS-INNES, C. S., SHANNON, N., LYNCH, A. G., FORSHEW, T., BARBERA, M., MURTAZA, M., ONG, C. J., LAO-SIRIEIX, P., DUNNING, M. J. et al.. 2014. Ordering of mutations in preinvasive disease stages of esophageal carcinogenesis. *Nat Genet,* 46**,** 837-843.

WILLIAMS, D. 2008. Radiation carcinogenesis: lessons from Chernobyl. *Oncogene,* 27 Suppl 2**,** S9-18.

WILTSHIRE, J. J., DRAKE, T. M., UTTLEY, L. & BALASUBRAMANIAN, S. P. 2016. Systematic Review of Trends in the Incidence Rates of Thyroid Cancer. *Thyroid,* 26**,** 1541-1552.

XING, M. 2005. BRAF mutation in thyroid cancer. *Endocr Relat Cancer,* 12**,** 245-62.

XING, M. 2013. Molecular pathogenesis and mechanisms of thyroid cancer. *Nat Rev Cancer,* 13**,** 184-99.

718 XING, M. 2016. Clinical utility of RAS mutations in thyroid cancer: a blurred picture now
719 emerging clearer. *BMC Med,* 14**,** 12.
720 YAPA, S., MULLA, O., GREEN, V., ENGLAND, J. & GREENMAN, J. 2017. The Role of
721 Chemokines in Thyroid Carcinoma. *Thyroid,* 27**,** 1347-1359.
722 YE, L., ZHOU, X., HUANG, F., WANG, W., QI, Y., XU, H., YANG, S., SHEN, L., FEI, X., XIE, J., CAO,
723 M., ZHOU, Y., ZHU, W., WANG, S., NING, G. & WANG, W. 2017. The genetic
724 landscape of benign thyroid nodules revealed by whole exome and transcriptome
725 sequencing. *Nat Commun,* 8**,** 15533.
726 ZABLOTSKA, L. B., BOGDANOVA, T. I., RON, E., EPSTEIN, O. V., ROBBINS, J., LIKHTAREV, I. A.,
727 HATCH, M., MARKOV, V. V., BOUVILLE, A. C., OLIJNYK, V. A. et al.. 2008. A cohort
728 study of thyroid cancer and other thyroid diseases after the Chornobyl accident:
729 dose-response analysis of thyroid follicular adenomas detected during first
730 screening in Ukraine (1998-2000). *Am J Epidemiol,* 167**,** 305-12.
731 ZANE, M., SCAVO, E., CATALANO, V., BONANNO, M., TODARO, M., DE MARIA, R. & STASSI, G.
732 2016. Normal vs cancer thyroid stem cells: the road to transformation. *Oncogene,*
733 35**,** 805-15.
734

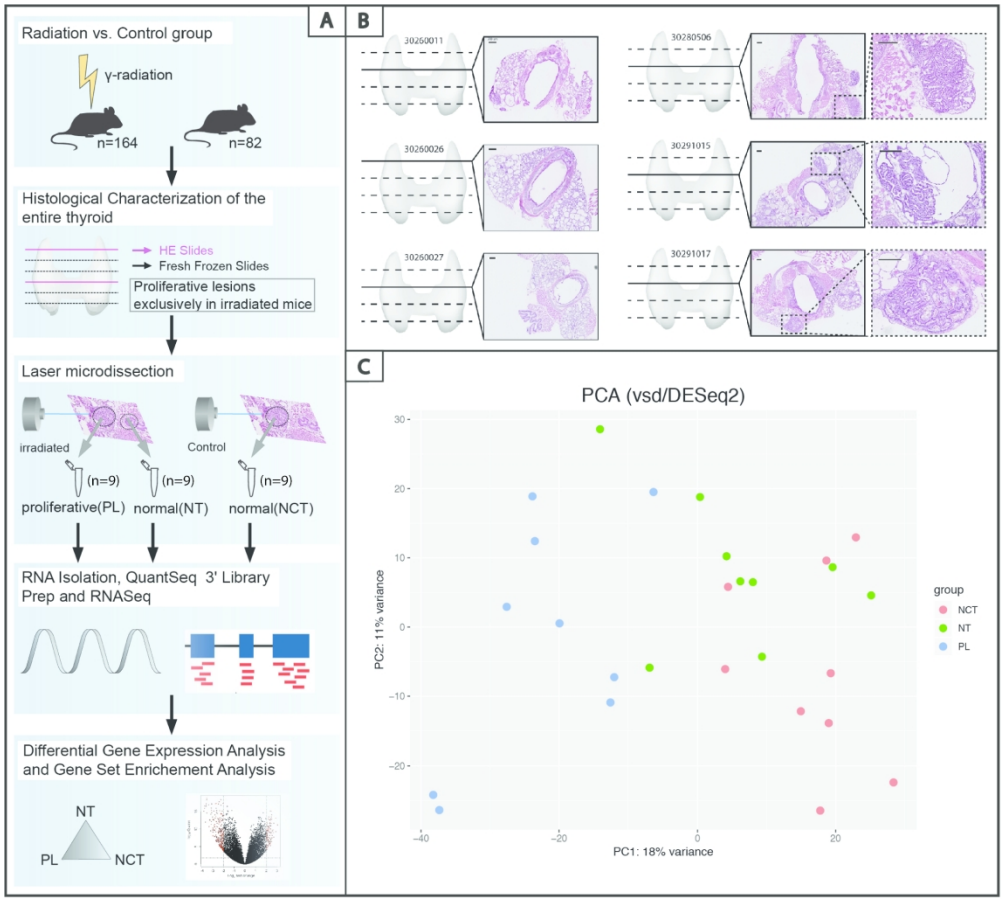

Figure 1: Panel A: Workflow of the study. Panel B: Examples of thyroid HE-sections and histological examination (all samples in SI Figure 1). Panel C: Principal component analysis of RNAseq data (vst counts) generated from the three histological groups.

190x170mm (300 x 300 DPI)

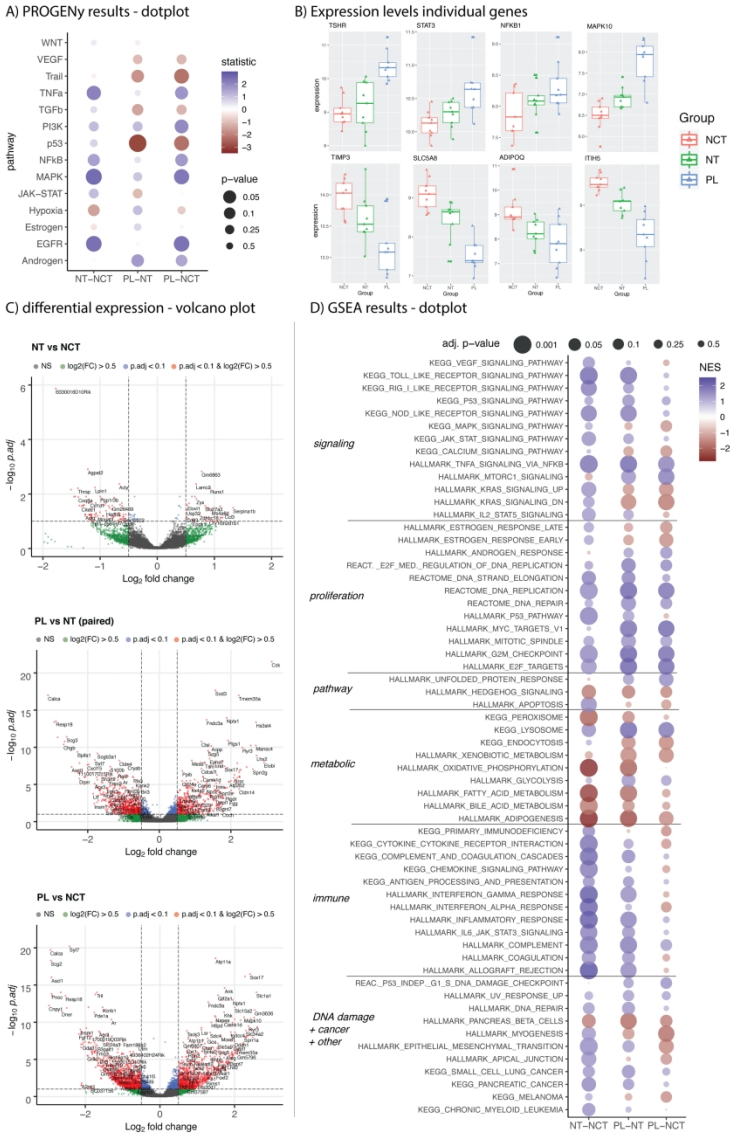

Figure 2: Transcriptomic analysis results
Panel 2A: Dot plot of PROGENy results: All pathways included in PROGENy were visualized. Dot size corresponds to signal strength (bigger is stronger), dot color reflects the direction of the deregulation (red: down-regulated, blues: upregulated). Panel 2B: Box plots of gene expression (vst-counts/DESeq2) for a set of eight selected genes in the three histological groups.
Panel 2C: Volcano plot of differential gene expression analysis. Panel 2D: Dot plot of Gene Set Enrichment Analysis (GSEA) results. Dot size corresponds to -log2(adj-p-value) [lager dot = smaller adj-p-value], dot color reflects the Normalized Enrichment Score (NES) [red: downregulated, blue: upregulated].
NCT: histologically normal tissue from non-exposed mice
NT: histologically normal tissue from exposed mice that harbor proliferative lesions
PL: proliferative lesions tissue from exposed mice

200x301mm (300 x 300 DPI)

SI Figure 1: Page 1: Microscopic images of HE sections and location of proliferative lesions within the thyroid gland (scale bar = 200 µm)

(figure legend on page 3)

SFigure 1: Page 2/3: Visualization of immune cell densities (figure legend on page 3)
(scale bar = 200 µm)

30260011

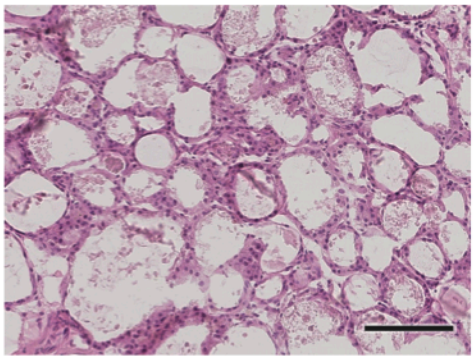

30280506

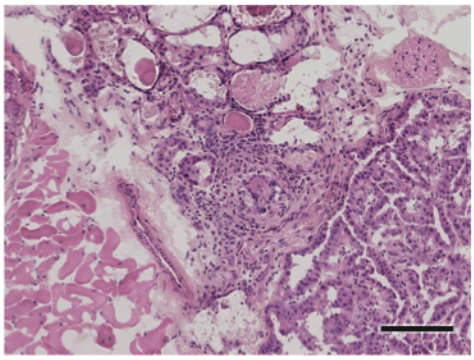

30260026

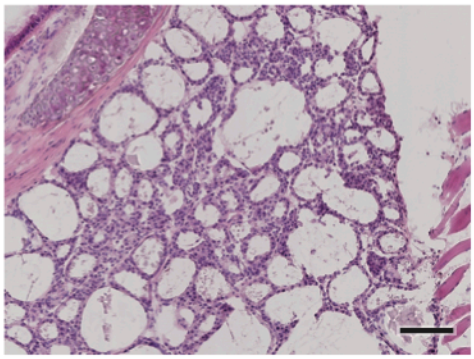

30291015

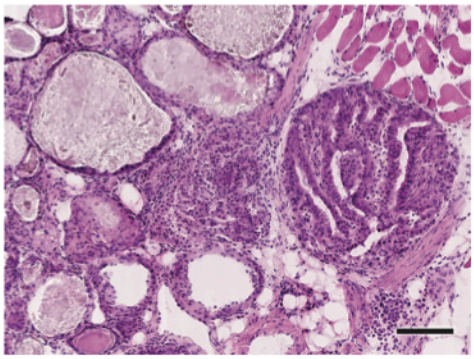

30260027

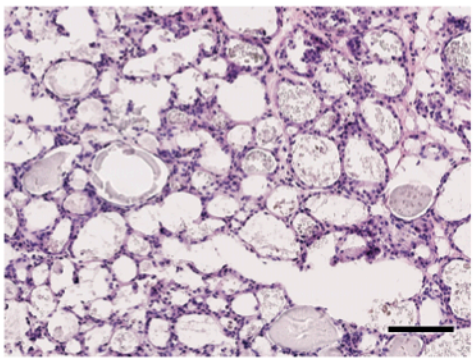

30291017

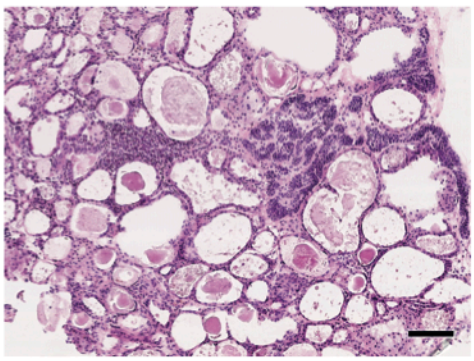

30266844

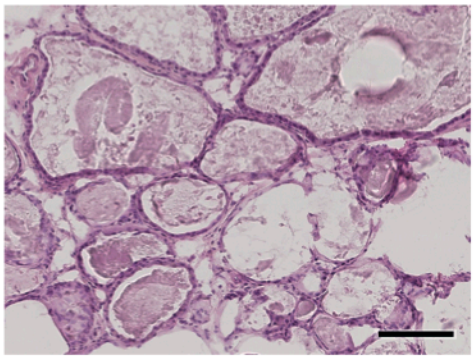

30298547

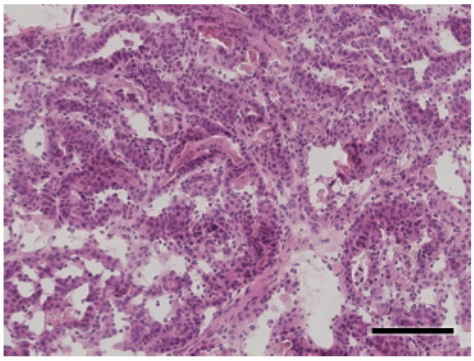

30291035

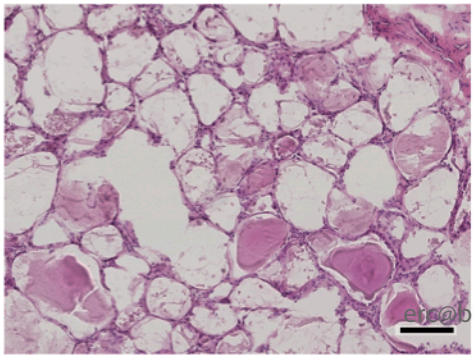

30280477

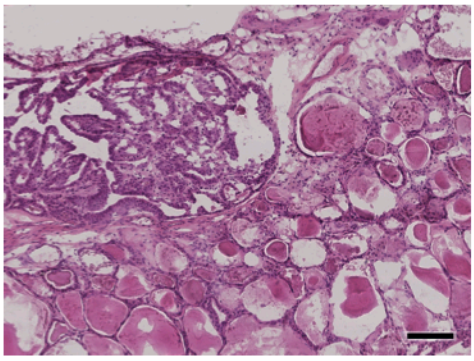

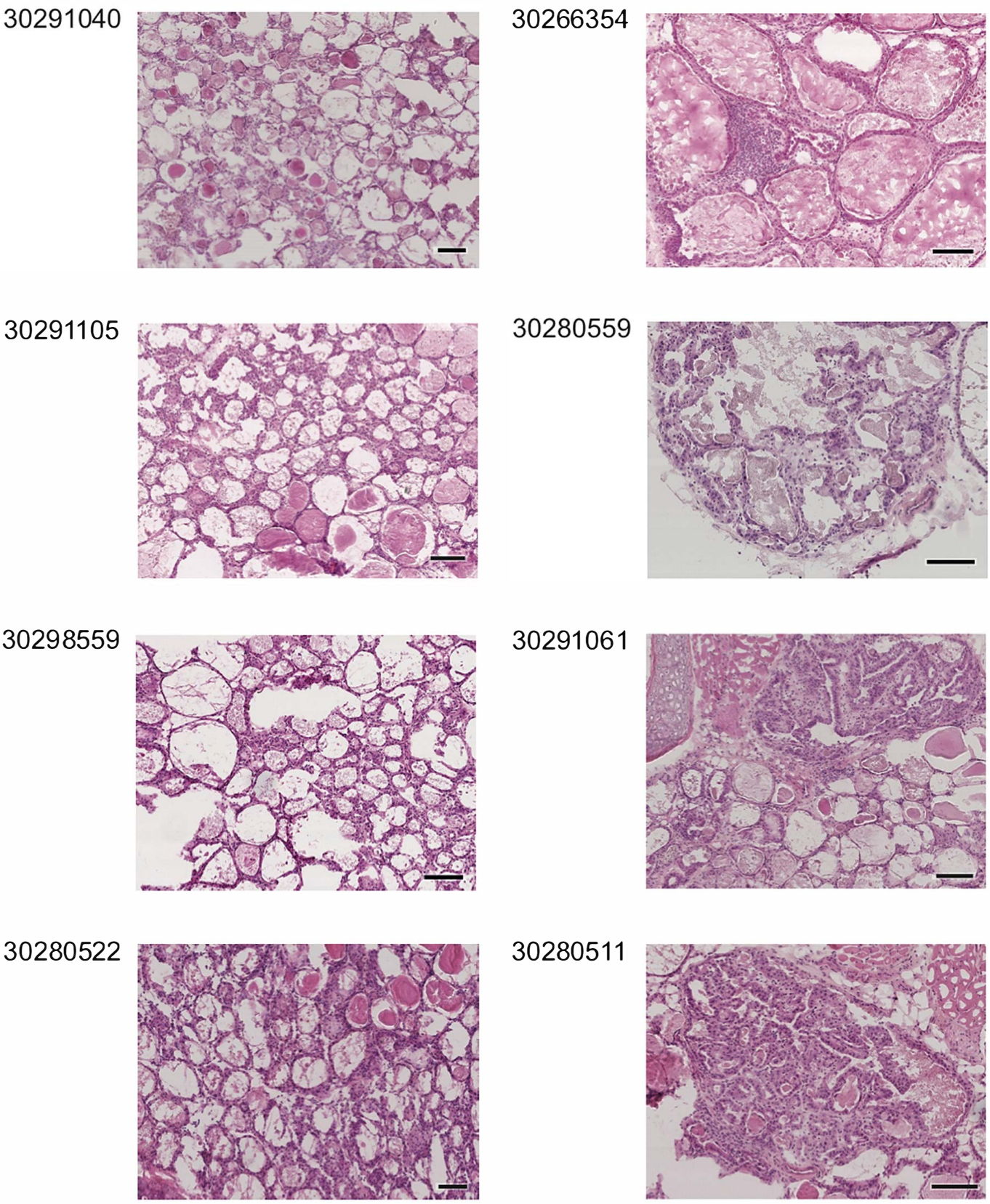

SI Figure 1

Page 1: The left column shows HE tissue sections derived from non-exposed mice without histological thyroid aberrations (9 samples/mice). The right column shows HE tissue sections from exposed mice that exhibited histological aberrations in the thyroid and their histological classifications (9 samples/ mice). Page 2/3: The left column shows exemplary tissue areas for the visualization of immune cell densities within the different tissues. The right column shows exposed cases harboring a histological aberration.

The scale bar (black) in each plot equals 200 micrometers.

SI Figure 2
Immune cells in histo–groups

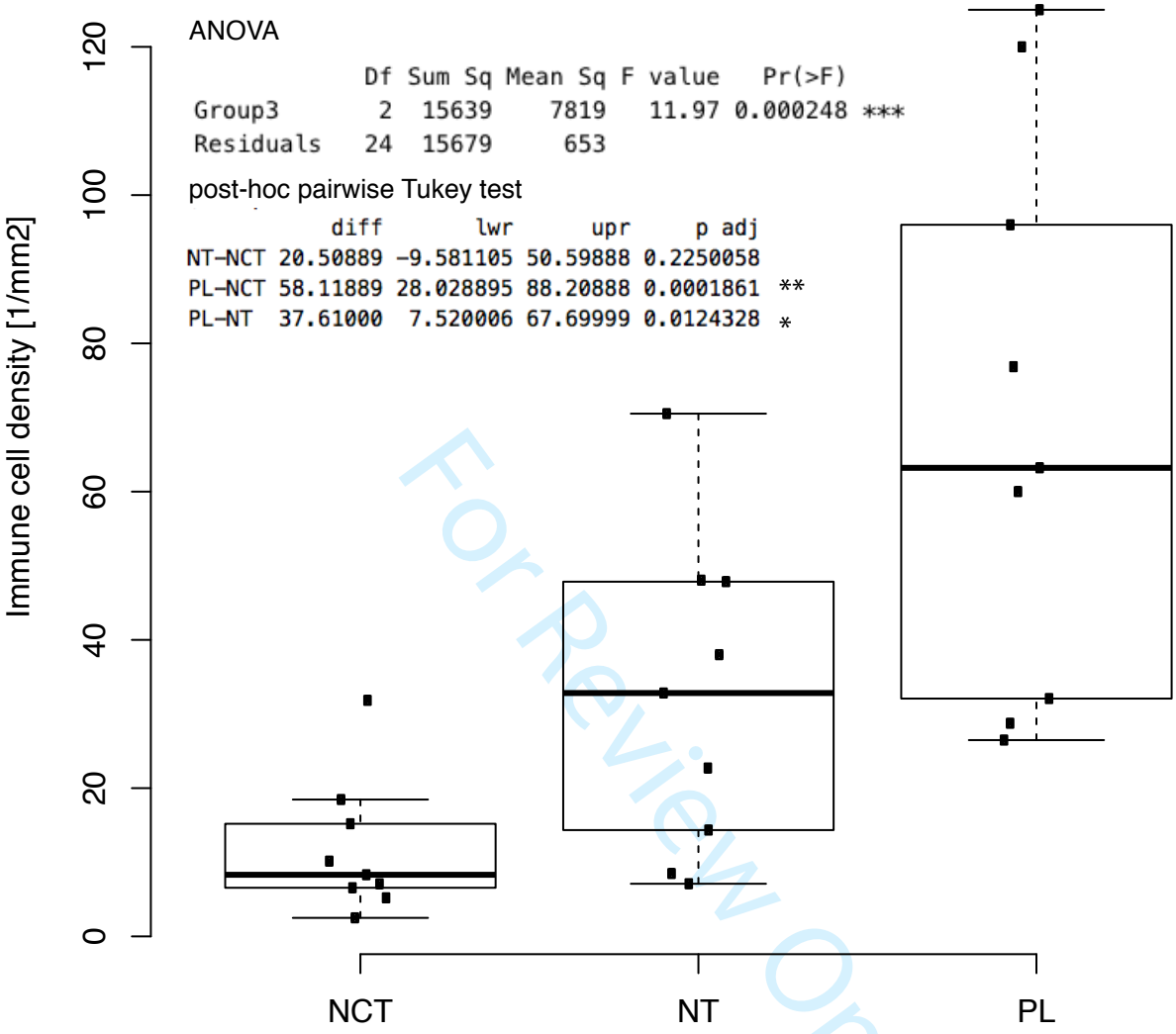

NCT: normal control tissue non-exposed mice, NT: normal tissue exposed mice
PL: proliferative lesions tissue exposed mice

Si Figure 2:
Box plots of immune cell densities observed in the different tissues by investigation of multiple tissue sections from each sample are shown. Statistically significant differences (p-adj < 0.05) were observed between PL and NCT tissues and between PL and NT tissues by ANOVA and post-hoc Tukey test.

A) **Clustering of samples by expression levels of thyroid cancer-associated genes (85 genes)**

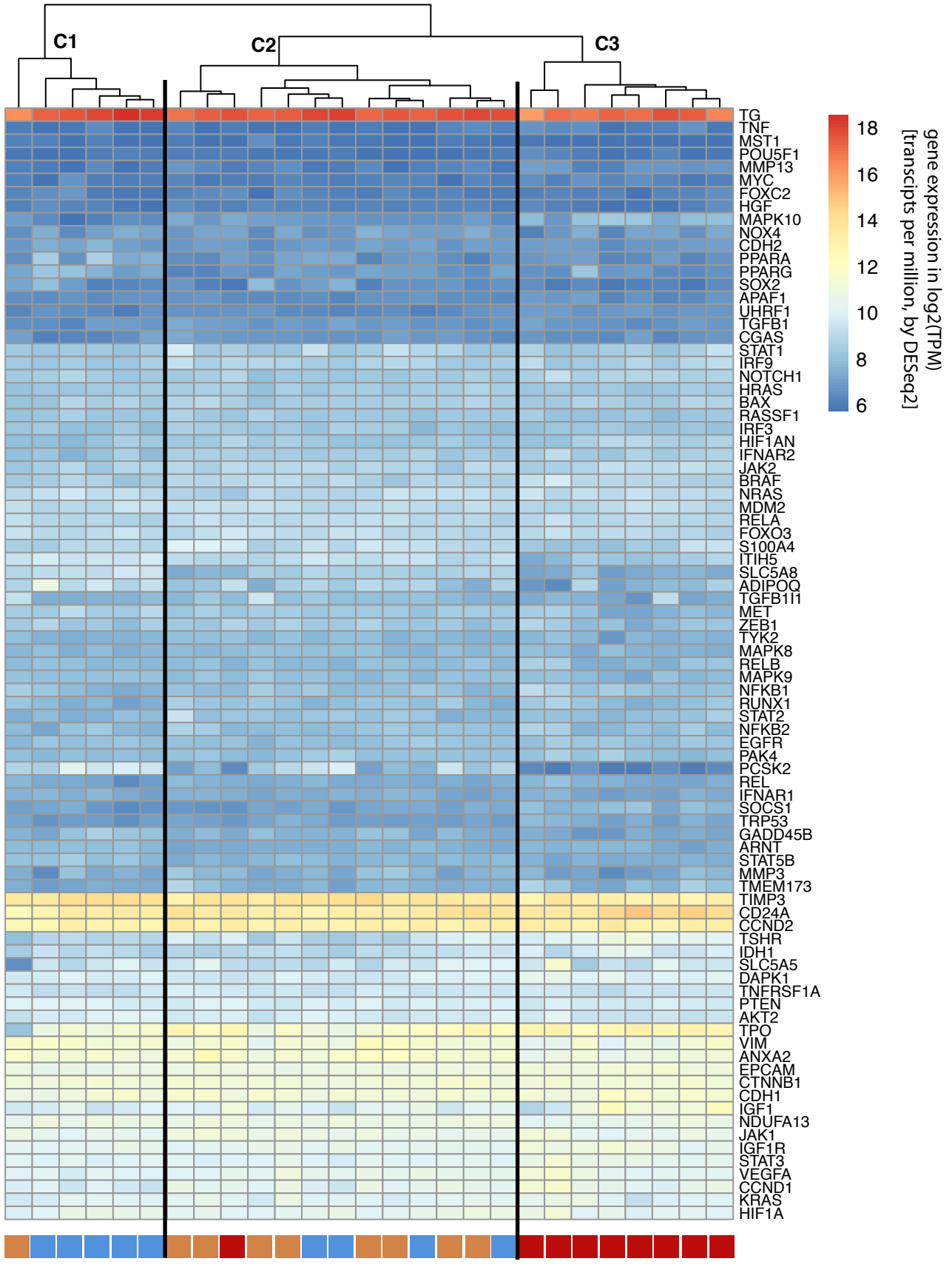

NCT: normal control tissue non-exposed mice
NT: normal tissue of exposed mice harboring PLs
PL: proliferative lesions tissue exposed mice

SI Figure 3A:
Hierarchical clustering of 27 tissue samples by their expression levels of 85 thyroid cancer-associated genes derived from the literature. The clustering results in three main clusters and separates the samples by tissue origin. C1 predominantly contains normal control tissues from non-exposed mice without thyroid aberrations. C2 predominantly contains samples of histologically normal tissue from exposed mice harboring a histological thyroid aberration. C3 exclusively contains samples from the proliferative lesions tissue present in exposed mice.

B) PCA of full expression set: colors indicate the histological group and shapes indicate the cluster based on SI Figure 3A

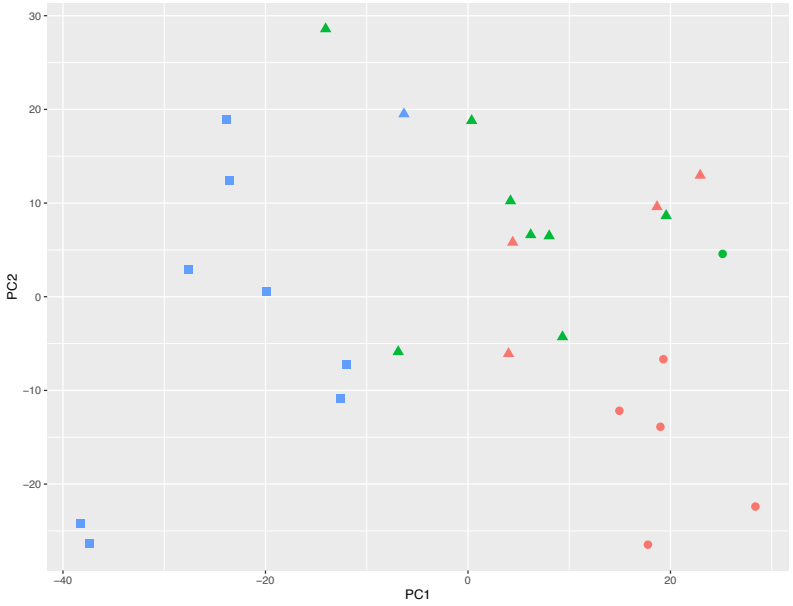

Scree Plot: Variance explained in each PC1 - PC10

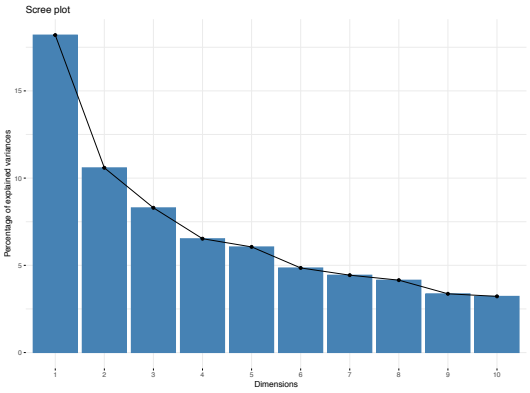

C) PCA of 500 top variant genes: colors indicate the histological group and shapes indicate the cluster based on SI Figure 3A

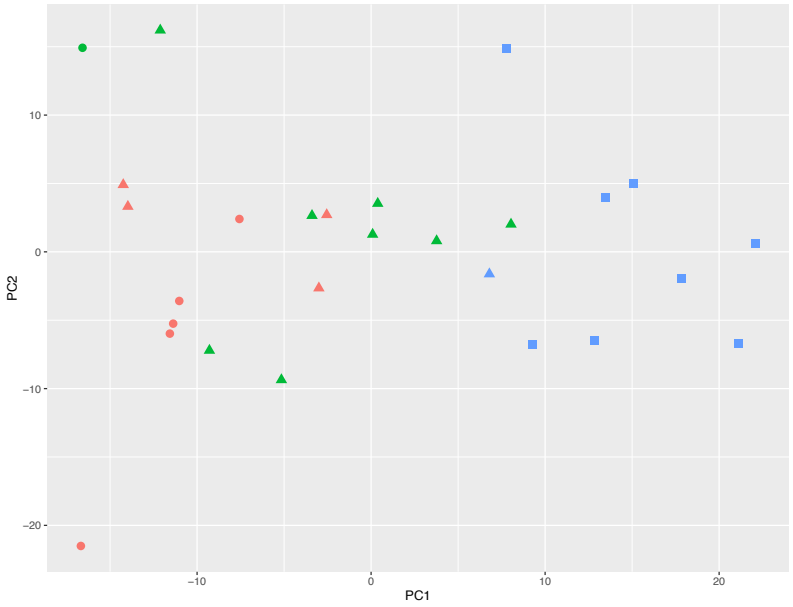

Scree Plot: Variance explained in each PC1 - PC10

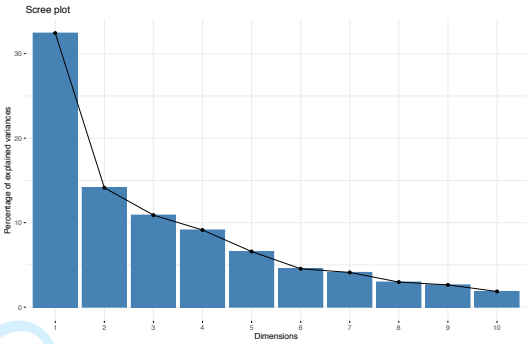

D) MDS of full expression set: colors indicate the histological group and shapes indicate the cluster based on SI Figure 3A

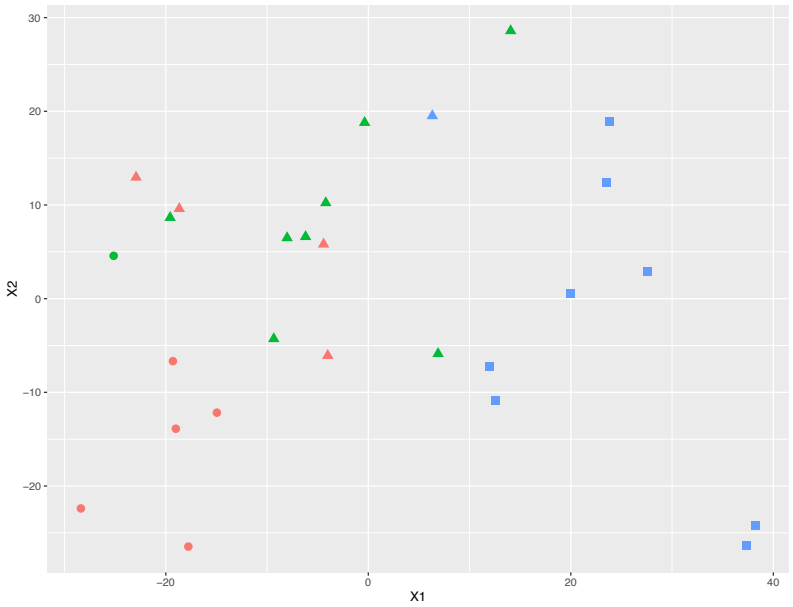

A)

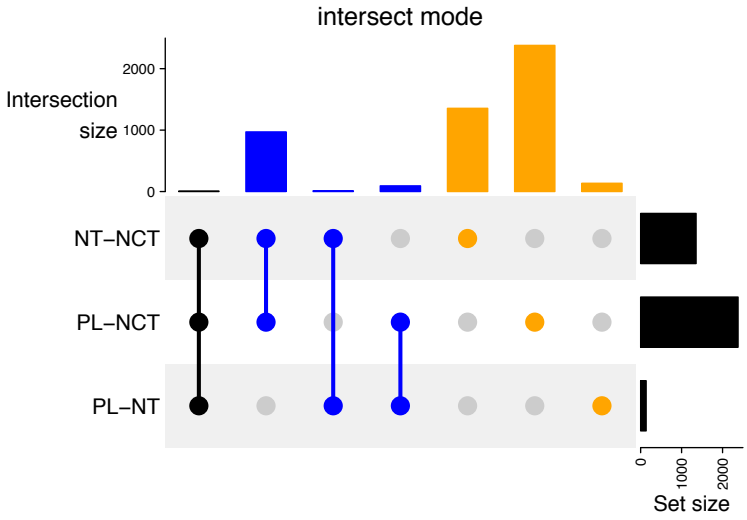

B)

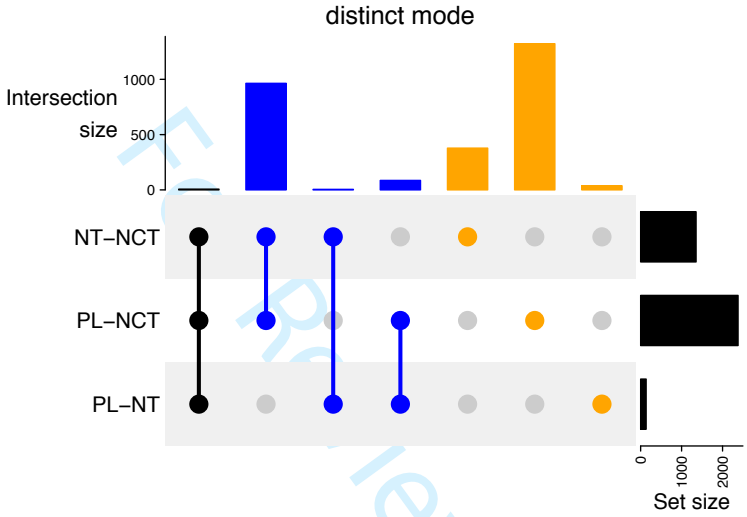

C)

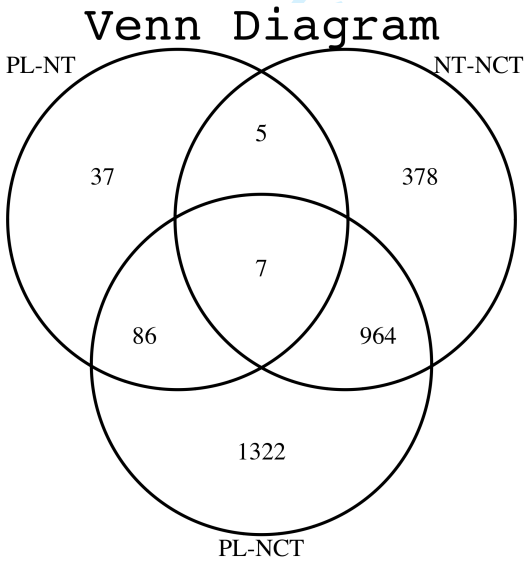

SI Figure 4: Upset and Venn plot differentially expressed genes
Panel A) Upset plot in intersect mode. Panel B) Upset plot in distinct mode Panel C) Venn diagram of differentially expressed genes

NCT: histologically normal tissue from non-exposed mice
NT: histologically normal tissue from exposed mice that harbor proliferative lesions
PL: proliferative lesions tissue from exposed mice

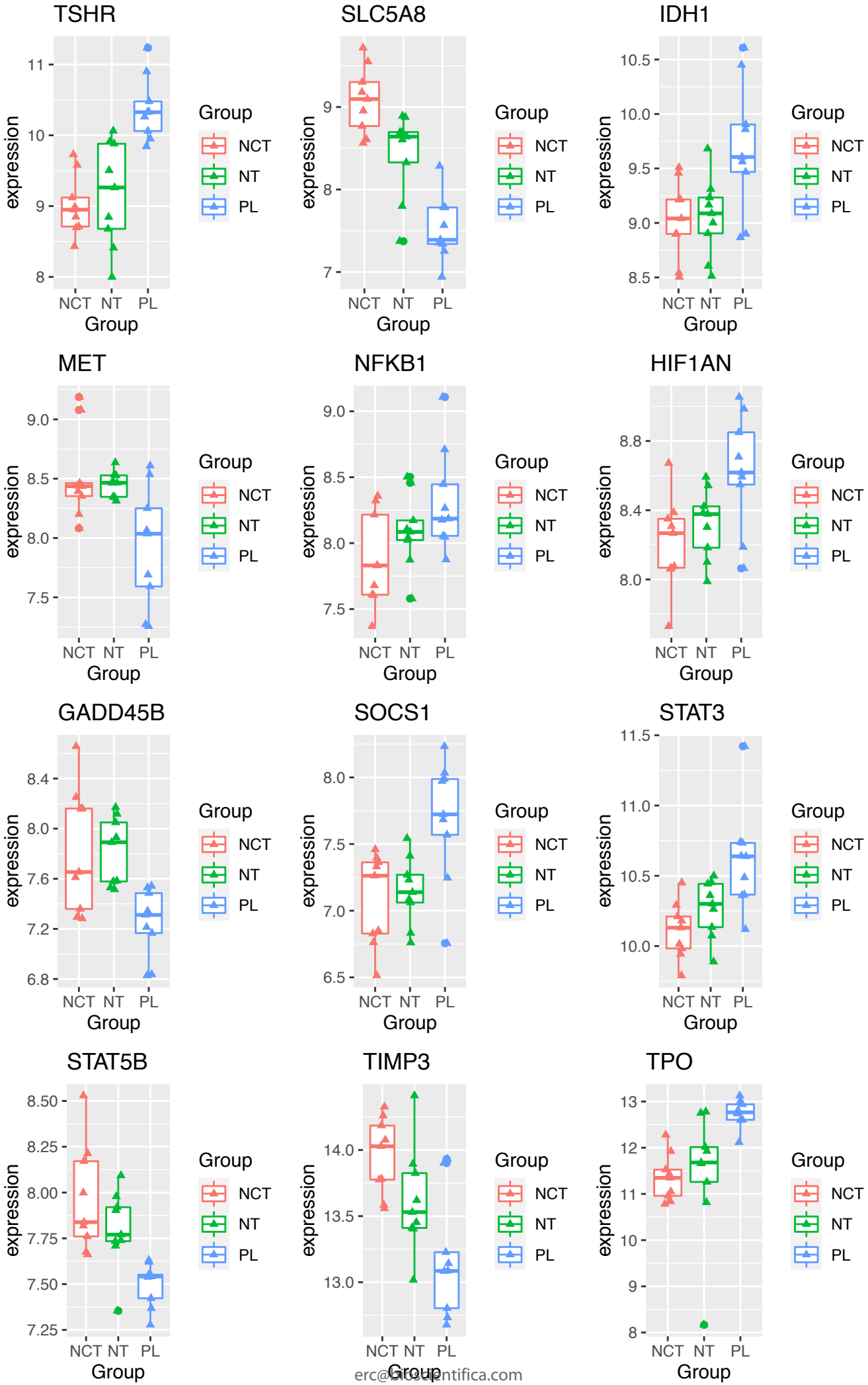

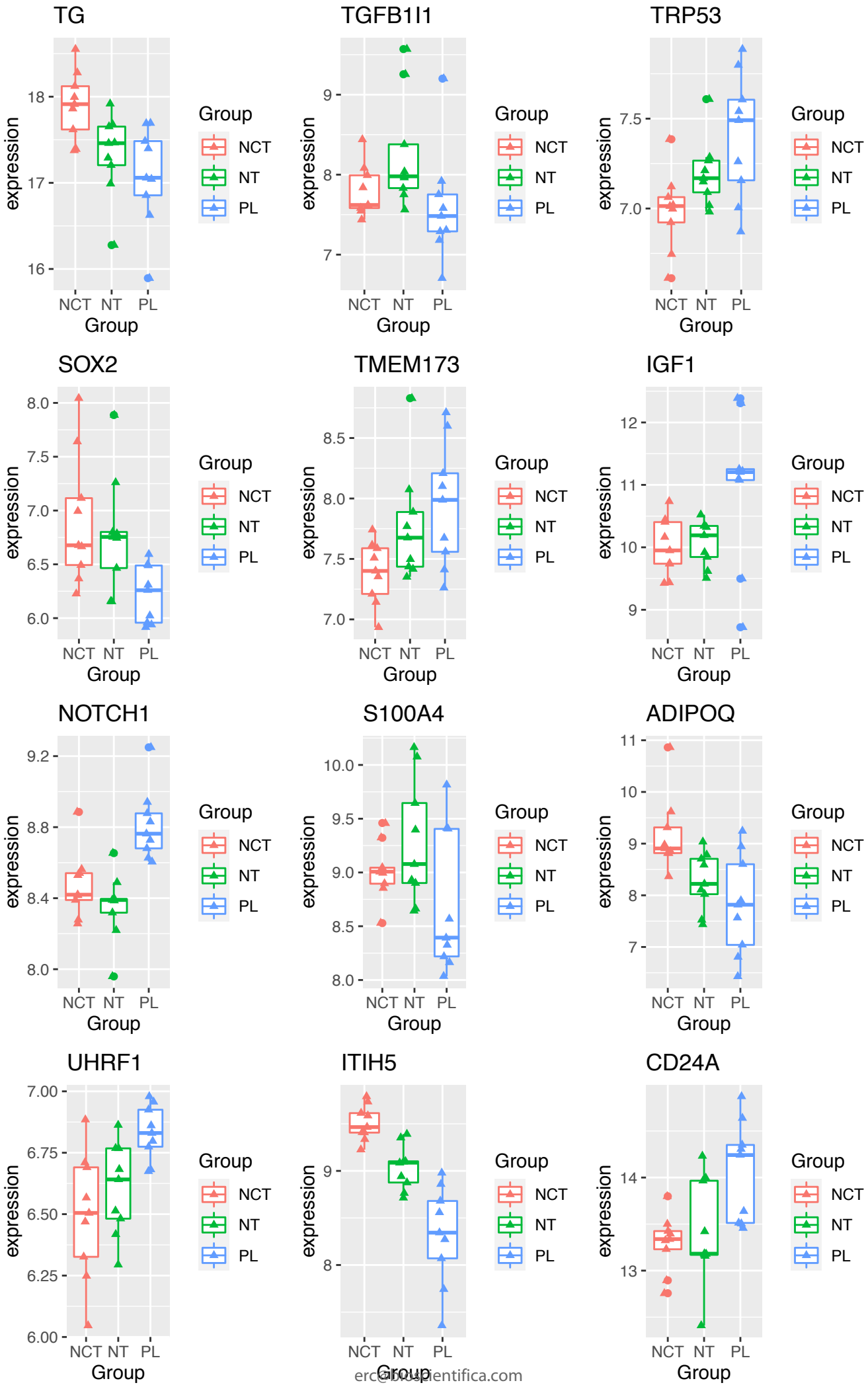

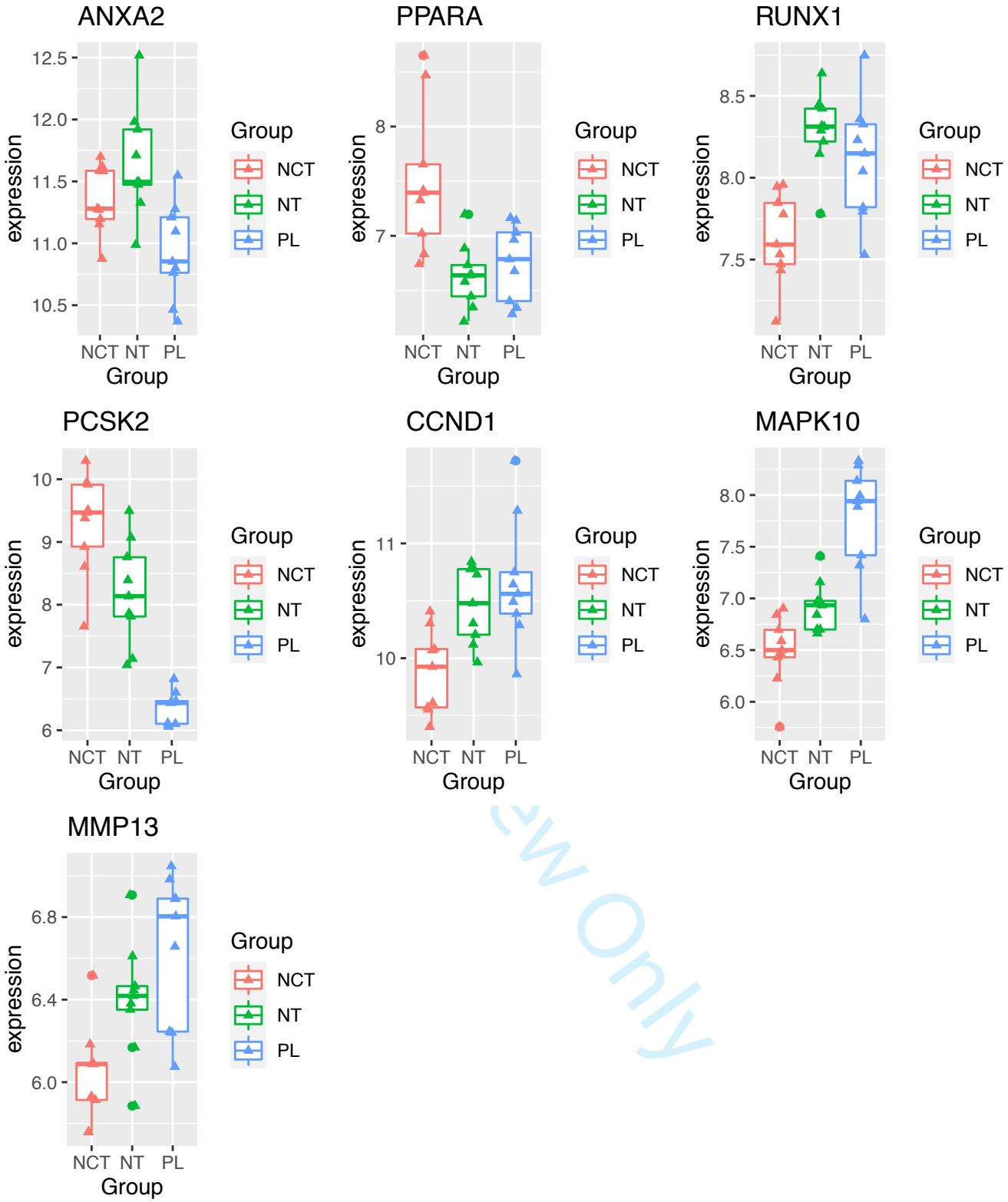

SI Figure 5:
TPM (transcripts per million) expression levels of thyroid cancer-associated genes derived from the literature (total 85 genes, SI Figure 3, SI Table 10). The visualized 31 genes were differentially expressed in at least one of the three group comparisons carried out (DESeq2). NCT: normal control tissue from mice with thyroid aberrations, NT: normal tissue from mice harboring PL tissue, PL: proliferative lesions tissue

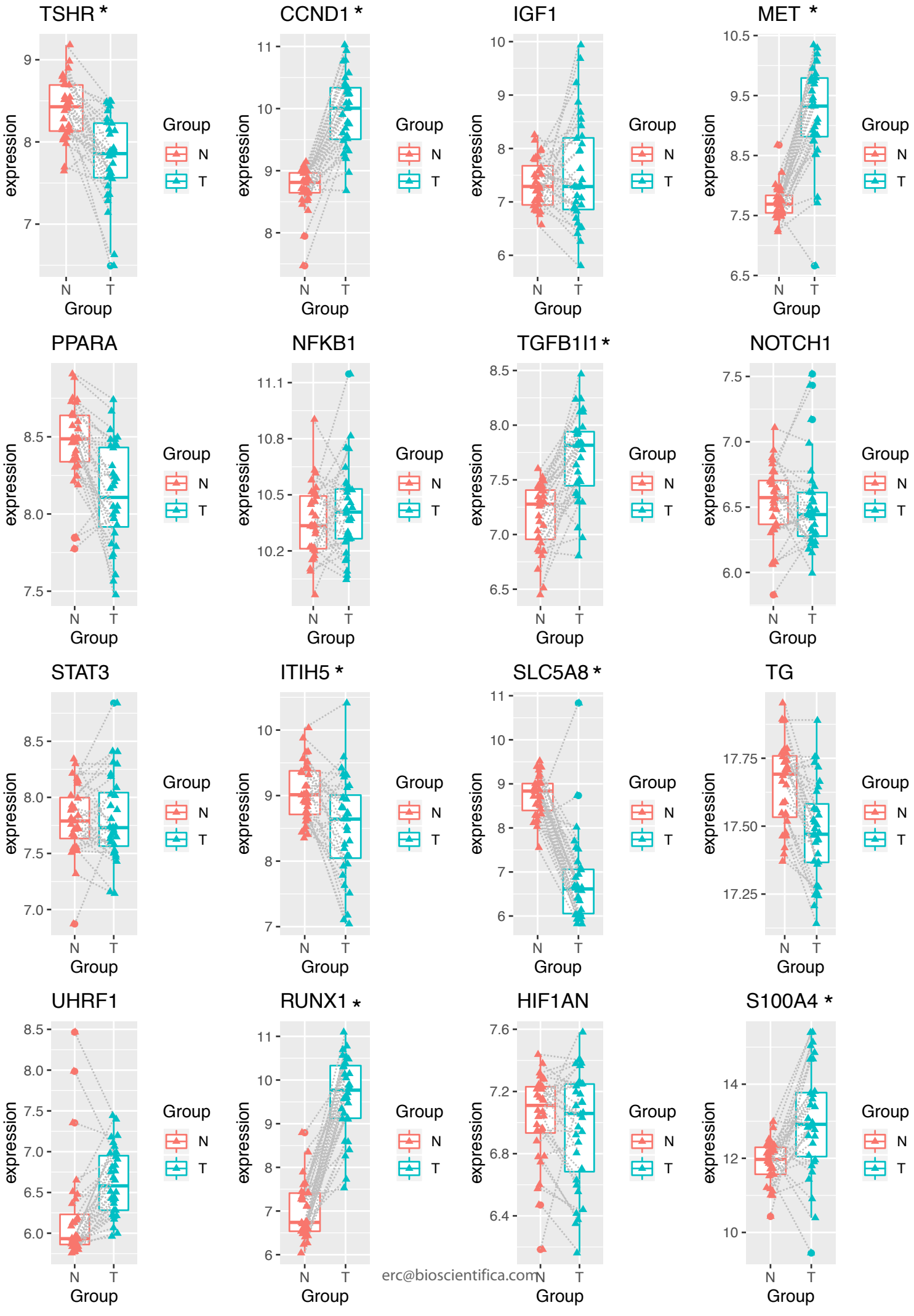

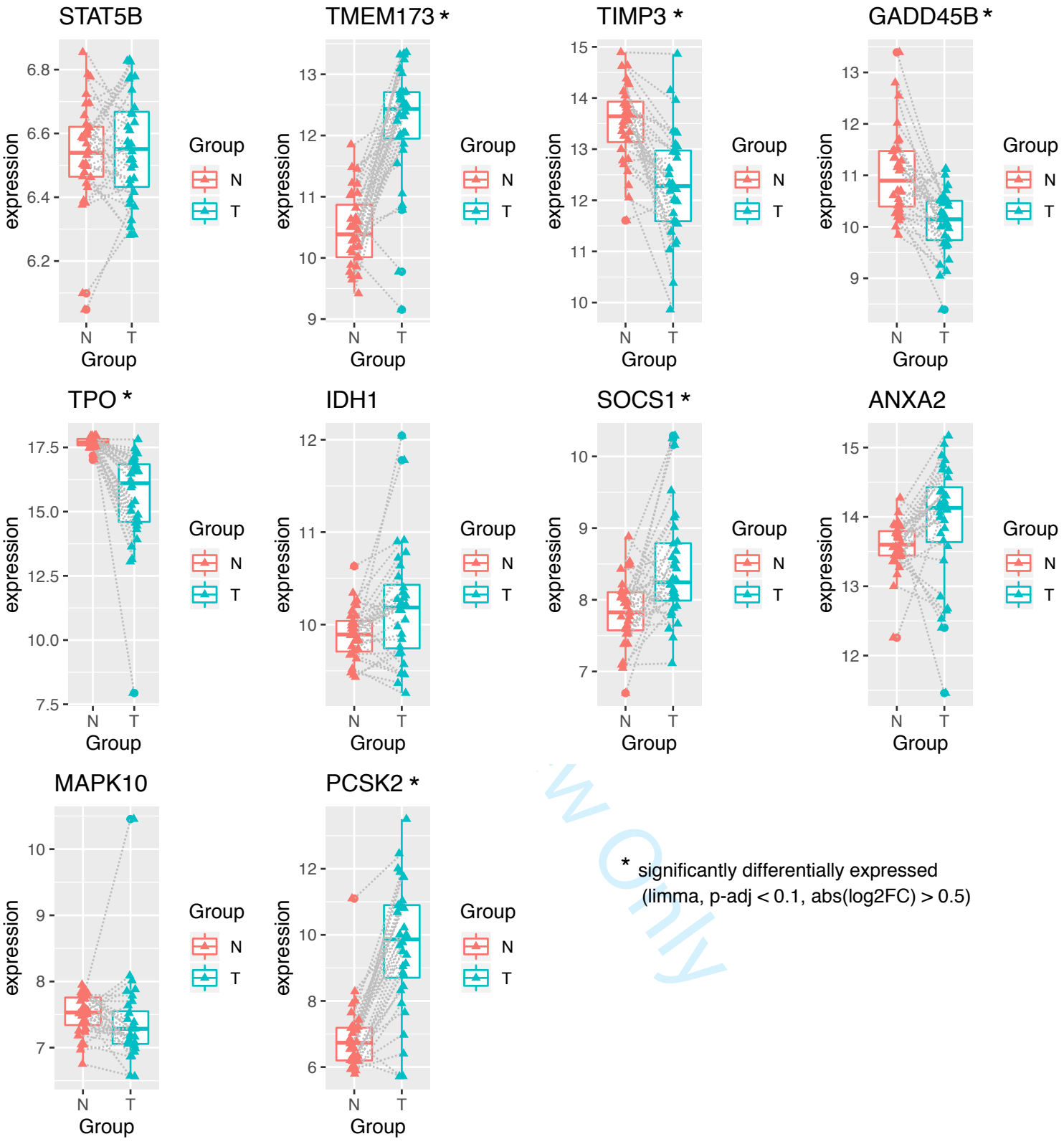

SI Figure 6 (page 1/2):
Gene expression levels (log2, Agilent 44K Array) in a human papillary thyroid carcinoma data set of the UkrAm post-chernobyl cohort. Expression levels of 26 genes are visualized in normal (N) and tumor (T) tissues. The 26 genes are a subset of the thyroid cancer-associated genes derived from the literature (n=85), which showed statistical significance in at least one out of of the three differential gene expression analysis comparisons made between proliferative lesions (PL), normal tissue (NT) and normal control tissue (NCT) of the investigated mice (SI Figure 5).
A transcriptomic differential expression analysis between normal and tumor tissue was carried out using the *limma* r package.
The results for the 26 genes are visualized in a volcano plot on page3.

Volcano–Plot: differential expression Tumor tissue vs Normal tissue

paired differential expression analysis (limma), human data / UkrAm cohort (Agilent 44K Arrays)

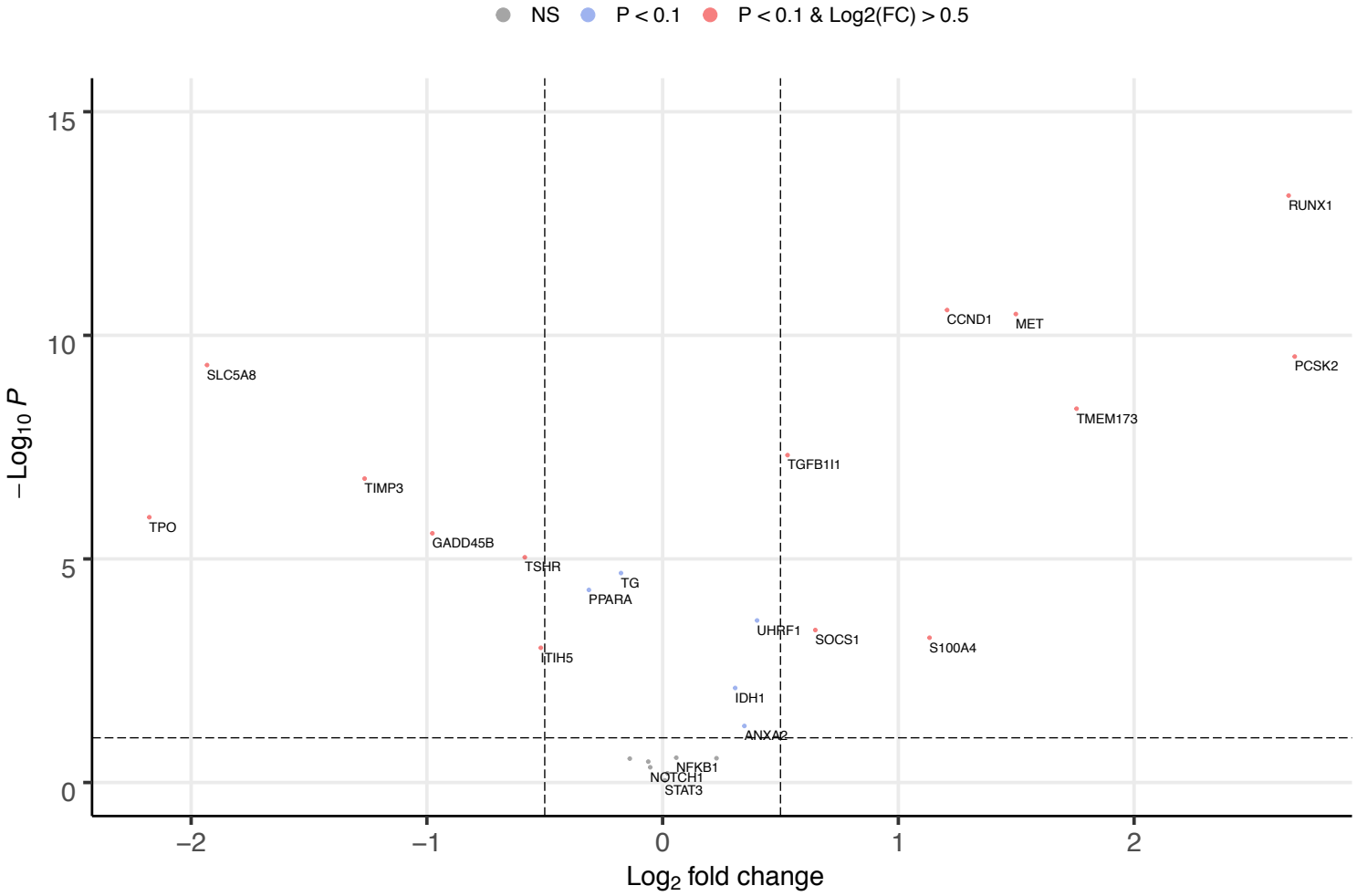

Total = 26 variables

SI Table 2: Sample Information

Mouse ID	sex	type	dose	age	Histological features									Inflammatory activity (lymphocytes per mm²)		Classification
					well demarcated	Compression	Capsule	Infiltration	Pattern	Cells	Nuclei	Epithelium	Follicles	neoplasia	normal	
30280477	m	wildtype	0.125 Gy	24 months	no	none	partially	none	papillary	low columnar	round	single layered/pseudostratified	enlarged	28.75	8.48	Follicular Hyperplasia
30280506	f	wildtype	0.125 Gy	24 months	yes	none	partially	none	papillary	cuboidal	oval	single layered	variable	60	32.83	Follicular Adenoma
30291015	f	wildtype	0.063 Gy	24 months	partially	partially	partially	none	papillary	cuboidal	oval	single layered	variable	76.85	47.85	Follicular Hyperplasia
30291017	f	wildtype	0.063 Gy	24 months	yes	none	yes	none	papillary	cuboidal	round	single layered/pseudostratified	enlarged/variable	96	70.52	Follicular Adenoma
30298547	m	B6RCF1 (het mut)	0.125 Gy	18 months	yes	partially	partially	none	solid	cuboidal	round/elongated	single layered/pseudostratified	/	26.48	7.1	Follicular Adenoma
30266354	f	wildtype	0.5 Gy	18 months	no	none	none	none	papillary	columnar	oval	single layered	enlarged	63.21	48.05	Follicular Hyperplasia
30280511	f	wildtype	0.125 Gy	24 months	yes	none	partially	none	papillary/solid	cuboidal	oval	single layered	variable	120	14.34	Follicular Hyperplasia
30280559	f	B6RCF1 (het mut)	0.125 Gy	24 months	no	none	none	none	papillary	cuboidal	round	single layered	variable	32.08	38	Follicular Hyperplasia
30291061	m	B6RCF1 (het mut)	0.063 Gy	24 months	no	none	partially	none	papillary	columnar	oval	single layered	variable	125	22.71	Follicular Hyperplasia
30260011	f	B6RCF1 (het mut)	sham (0 Gy)	24 months		none	/	none		cuboidal	oval	single layered	variable		5.2	Normal thyroid tissue
30260026	f	wildtype	sham (0 Gy)	24 months		none	/	none		cuboidal	round/normal	single layered	variable		31.84	Normal thyroid tissue
30260027	f	wildtype	sham (0 Gy)	24 months		none	/	none		cuboidal/squamous		single layered	variable		8.31	Normal thyroid tissue
30266844	f	wildtype	sham (0 Gy)	18 months		none	/	none		squamous	oval	single layered	variable/enlarged		10.15	Normal thyroid tissue
30280522	f	wildtype	sham (0 Gy)	24 months		none	/	none		cuboidal	round/oval	single layered	variable		18.46	Normal thyroid tissue
30291035	m	wildtype	sham (0 Gy)	24 months		none	/	none		squamous	oval	single layered	variable		6.56	normal thyroid tissue
30291040	f	wildtype	sham (0 Gy)	24 months		none	/	none		cuboidal/squamous	oval	single layered	variable		7.09	Normal thyroid tissue
30291105	m	B6RCF1 (het mut)	sham (0 Gy)	24 months		none	/	none		cuboidal	round	single layered	variable		15.19	Normal thyroid tissue
30298559	m	B6RCF1 (het mut)	sham (0 Gy)	18 months		none	/	none		cuboidal/squamous		single layered	normal		2.5	Normal thyroid tissue

SI Table 3: RNA quality control

Sample_Name	**DV200 [%]**	**RIN**	Experimental Group
30260011	99	6.8	normal
30260026	97	5.4	normal
30260027	98	7.6	normal
30266354	98	7.1	normal
30266354 P	97	6	papillary
30280477 P	96	5.1	papillary
30280477	96	4	normal
30268844	95	8.2	normal
30280506	95	3.3	normal
30280506 P	96	5.2	papillary
30280511 P	97	4.8	papillary
30280511	96	4	normal
30280522	98	N/A	normal
30280559	97	5.1	normal
30280559 P	96	4.3	papillary
30291015 P	94	7.2	papillary
30291015	97	5.5	normal
30291017	93	4.7	normal
30291017 P	94	7.4	papillary
30291061 P	98	7.1	papillary
30291061	97	6.7	normal
30291035	96	6.4	normal
30291040	97	7.9	normal
30291105	96	4.8	normal
30298547	96	5.7	normal
30298547 P	96	6.4	papillary
30298559	96	5.4	normal

SI Table 5: qRT-PCR validation

Gene	r (pearson)	differentially expressed	qRT-Probe [bp, exons, amplicon length)	total No. of exons	Forward primer seq	Reverse primer seq
ALAS1	0.82	FALSE	1591-1681 (exon 8-9) 95bp	12	ATCATCCCTGTGCGGGTTG	TAATTGATGGCCTGGACGTAGATATT
CD36	0.91	TRUE	809-870 (exon 8-9) 62bp	18	ACATTTGCAGGTCTATCTACGCTG	CACGGGGATTCCTTTAAGGTC
HSP90AA1	0.21	TRUE	151-229 (exon 1-2) 79bp	11	AATTCATCGGACGCTCTGGA	GCAGCTCCTTCCCCGAGT
IL1B	0.84	TRUE	42-112 (coding exon 1-3) 71bp	7	TGACAGTGATGAGAATGACCTGTTC	AGGTTTGGAAGCAGCCCTTC
LRP1	0.89	FALSE	13182-13245 (exon85-86) 64bp	90	GATGCCTGAGTGCCAGTGC	ACTAACAACCTGCTCCTCGCA
PLAU	0.53	FALSE	672-743 (exon 6-7) 72bp	12	CGCACACTGCTTCATTCAACTC	GAGCTCTCCTTCGACTGACCC
SERPINE1	0.66	TRUE	1072-1109 (exon 6-7) 38bp	9	GCGTCTTCCTCCACAGCCT	ATGCGGGCTGAGATGACAA
THBS1	0.82	FALSE	2739-2783 (exon 16-17) 45bp	22	GGTGCCCAATCCTGACCAG	CCTCGGCCATCACCATCA

ɒ RNAseq quatifications (27 Samples)

SI Table 8: PROGENY results

Statistical results derived by PROGENy (pathway response gene analysis) (NTC: normal control tissues from non-exposed mice, NT: normal tissues from exposed mice harbouring proliferative lesions, PL: proliverative lesions tissues from exposed mice)

NT vs NCT				
pathway	**estimate**	**std.error**	**statistic**	**p.value**
WNT	0.195777053	0.431827524	0.45336863	0.656371541
VEGF	-0.006549149	0.492908874	-0.013286733	0.989563299
Trail	-0.227238901	0.723004129	-0.314298207	0.757355653
TNFa	1.13534352	0.458764067	2.474787374	0.024904424
TGFb	0.445795702	0.657997905	0.677503224	0.507765831
PI3K	0.586814989	0.437679251	1.34074208	0.198730493
p53	0.399395894	0.475650254	0.839683971	0.413456867
NFkB	0.931797749	0.492592228	1.891620891	0.076784886
MAPK	1.554670346	0.522317651	2.976484414	0.008905583
JAK-STAT	0.890521168	0.6712306	1.326699301	0.203233074
Hypoxia	-0.9010885	0.504838937	-1.784902937	0.093246705
Estrogen	-0.191998714	0.350699541	-0.547473526	0.591609157
EGFR	1.472880008	0.51360115	2.867750606	0.011163071
Androgen	-0.052879595	0.44530485	-0.118749201	0.906952183
PL vs NT				
WNT	-0.233372267	0.674931228	-0.345771921	0.734018674
VEGF	-0.506334131	0.401839623	-1.260040331	0.225723727
Trail	-1.122713494	0.551560455	-2.035522099	0.058709125
TNFa	0.385173214	0.736818804	0.522751608	0.608310522
TGFb	-0.752697994	0.442455121	-1.70118495	0.108257608
PI3K	0.82994821	0.615433736	1.348558198	0.1962592
p53	-1.658412711	0.478809447	-3.463617352	0.003200224
NFkB	0.371743796	0.622646643	0.597038145	0.558836665
MAPK	0.969519534	0.84735588	1.144170421	0.269382285
JAK-STAT	-0.558661252	0.428200058	-1.304673463	0.210458763
Hypoxia	0.471061518	0.373891849	1.259887104	0.225777589
Estrogen	0.370897092	0.468331941	0.791953441	0.439972091
EGFR	0.09083846	0.506749386	0.179257169	0.859986151
Androgen	0.971747336	0.484530884	2.005542614	0.062121695
PL vs NCT				
WNT	0.003577585	0.587131443	0.006093329	0.995213584
VEGF	-0.558112382	0.413369849	-1.350152612	0.19575812
Trail	-2.388167751	0.909121115	-2.626897243	0.01831134
TNFa	1.49956756	0.705131149	2.126650568	0.049357643
TGFb	-0.835262493	0.596932445	-1.399257989	0.180823313
PI3K	1.293036125	0.552183113	2.34167995	0.032465487
p53	-1.28875785	0.483253619	-2.666835383	0.016879037
NFkB	1.336268654	0.662216314	2.017873353	0.060696875
MAPK	2.724274841	0.997175599	2.73199108	0.014770556
JAK-STAT	-0.085930913	0.576032812	-0.149177115	0.883277989
Hypoxia	-0.365286065	0.384995274	-0.948806622	0.356830976

Estrogen	-0.070725282	0.350259147	-0.201922727	0.842522125
EGFR	1.57936172	0.557935173	2.830726212	0.012051935
Androgen	0.80790848	0.456226243	1.770850523	0.095631283

SI Table 10: tyroid pathogenesis/carcinogenesis-associated genes from literature

GENE	Functional group	Source / Literature / Title	pubmed
ADIPOQ	metabolism	Dossus et al. 2017. Adipokines and inflammation markers and r	https://pubmed.ncbi.nlm.nih.gov/29168186/
AKT2	proliferation	Revilla et al 2019. Cross-Talk between Inflammatory Mediators	https://pubmed.ncbi.nlm.nih.gov/31109060/
ANXA2	cellular growth,proliferation	Effects of CD147 gene silencing on protein expression of ANXA2	https://pubmed.ncbi.nlm.nih.gov/24742570/
APAF1	apoptosis	Kebebew et al. 2006. Diagnostic and prognostic value of cell-cy	https://pubmed.ncbi.nlm.nih.gov/16547620/
ARNT	metabolism	Revilla et al 2019. Cross-Talk between Inflammatory Mediators	https://pubmed.ncbi.nlm.nih.gov/31109060/
BAX	apoptosis	Faria et al. 2019 The Emerging Role of Estrogens in Thyroid Red	https://pubmed.ncbi.nlm.nih.gov/30728883/
BRAF	proliferation	Revilla et al 2019. Cross-Talk between Inflammatory Mediators	https://pubmed.ncbi.nlm.nih.gov/31109060/
CCND1	cellular growht, metabolism	Jeon et al. 2918. CCND1 Splice Variant as A Novel Diagnostic an	https://pubmed.ncbi.nlm.nih.gov/30428594/
CCND2	cell cycle	Xia et al. 2018. LncRNA CCND2-AS1 promotes proliferation, mig	https://pubmed.ncbi.nlm.nih.gov/29366479/
CD24A	cell adhesion	Rusinek et al. 2011 Gene expression profile of human thyroid ca	https://pubmed.ncbi.nlm.nih.gov/21798995/
CDH1	cell-cell adhesions,proliferation	Rusinek et al. 2011 Gene expression profile of human thyroid ca	https://pubmed.ncbi.nlm.nih.gov/21798995/
CDH2	cell-cell adhesions	Qiu et al. 2018. Identification of key genes and miRNAs markers	https://pubmed.ncbi.nlm.nih.gov/30414611/
CGAS	inflammation	Kwon et al. 2019 The cytosolic DNA-sensing cGAS-STING pathw	https://pubmed.ncbi.nlm.nih.gov/31852718/
CTNNB1	cell-cell adhesions	Revilla et al 2019. Cross-Talk between Inflammatory Mediators	https://pubmed.ncbi.nlm.nih.gov/31109060/
DAPK1	apoptosis	Xing 2013, Molecular pathogenesis and mechanisms of thyroid	https://pubmed.ncbi.nlm.nih.gov/23429735/
EGFR	proliferation	Xing 2013, Molecular pathogenesis and mechanisms of thyroid	https://pubmed.ncbi.nlm.nih.gov/23429735/
EPCAM	cell-cell adhesions	Rusinek et al. 2011 Gene expression profile of human thyroid ca	https://pubmed.ncbi.nlm.nih.gov/21798995/
FOXC2	proliferation	Revilla et al 2019. Cross-Talk between Inflammatory Mediators	https://pubmed.ncbi.nlm.nih.gov/31109060/
FOXO3	cell growth	Revilla et al 2019. Cross-Talk between Inflammatory Mediators	https://pubmed.ncbi.nlm.nih.gov/31109060/
GADD45B	apoptosis	Pacifico et al. 2004 Oncogenic and anti-apoptotic activity of NF-	https://pubmed.ncbi.nlm.nih.gov/15475567/
HGF	cell growth	Revilla et al 2019. Cross-Talk between Inflammatory Mediators	https://pubmed.ncbi.nlm.nih.gov/31109060/
HIF1A	hypoxia	Revilla et al 2019. Cross-Talk between Inflammatory Mediators	https://pubmed.ncbi.nlm.nih.gov/31109060/
HIF1AN	hypoxia	Kebebew et al. 2006. Diagnostic and prognostic value of cell-cy	https://pubmed.ncbi.nlm.nih.gov/16547620/
HRAS	cell growth	Yoo et al. Comprehensive Analysis of the Transcriptional and M	https://pubmed.ncbi.nlm.nih.gov/27494611/
IDH1	cell cycle	Yoo et al. Comprehensive Analysis of the Transcriptional and M	https://pubmed.ncbi.nlm.nih.gov/27494611/
IFNAR1	proliferation	Sprooten et al. 2019. Type I interferons and dendritic cells in ca	https://pubmed.ncbi.nlm.nih.gov/31810554/
IFNAR2	proliferation	Sprooten et al. 2019. Type I interferons and dendritic cells in ca	https://pubmed.ncbi.nlm.nih.gov/31810554/
IGF1	metabolism	Giuliani et al. 2018. The Role of the Transcription Factor Nuclea	https://pubmed.ncbi.nlm.nih.gov/30186235/
IGF1R	metabolism	Giuliani et al. 2018. The Role of the Transcription Factor Nuclea	https://pubmed.ncbi.nlm.nih.gov/30186235/

IRF3	inflammation	Biswas et al. 2006. A distinct and unique transcriptional prograr	https://pubmed.ncbi.nlm.nih.gov/16269622/
IRF9	proliferation	Hu et al. 2018 STAT1 facilitates oestrogen receptor α transcripti	https://pubmed.ncbi.nlm.nih.gov/30334368/
ITIH5	tumour suppressor gene	Sasaki et al. 2017 Genome-wide in vivo RNAi screen identifies I1	https://pubmed.ncbi.nlm.nih.gov/28289921/
JAK1	proliferation	Vella et al. 2018. The Emerging Role of Insulin Receptor Isoform	https://pubmed.ncbi.nlm.nih.gov/30513575/
JAK2	proliferation	Revilla et al 2019. Cross-Talk between Inflammatory Mediators	https://pubmed.ncbi.nlm.nih.gov/31109060/
KRAS	proliferation	Yoo et al. Comprehensive Analysis of the Transcriptional and M	https://pubmed.ncbi.nlm.nih.gov/27494611/
MAPK10	proliferation	Revilla et al 2019. Cross-Talk between Inflammatory Mediators	https://pubmed.ncbi.nlm.nih.gov/31109060/
MAPK8	proliferation	Revilla et al 2019. Cross-Talk between Inflammatory Mediators	https://pubmed.ncbi.nlm.nih.gov/31109060/
MAPK9	proliferation	Revilla et al 2019. Cross-Talk between Inflammatory Mediators	https://pubmed.ncbi.nlm.nih.gov/31109060/
MDM2	tumour suppressor gene	Malaguarnera et al. TAp73 alpha increases p53 tumor suppress	https://pubmed.ncbi.nlm.nih.gov/18234963/
MET	proliferation	Rusinek et al. 2011 Gene expression profile of human thyroid ca	https://pubmed.ncbi.nlm.nih.gov/21798995/
MMP13	extracellular matrix	Rusinek et al. 2011 Gene expression profile of human thyroid ca	https://pubmed.ncbi.nlm.nih.gov/21798995/
MMP3	extracellular matrix	Rusinek et al. 2011 Gene expression profile of human thyroid ca	https://pubmed.ncbi.nlm.nih.gov/21798995/
MST1	cell growth	Xing 2013, Molecular pathogenesis and mechanisms of thyroid	https://pubmed.ncbi.nlm.nih.gov/23429735/
MYC	proliferation	Ye et al. 2020. Oncogenic Role of Long Noncoding RNAMALAT1	https://pubmed.ncbi.nlm.nih.gov/33312756/
NDUFA13	cell cycle	Xing 2013, Molecular pathogenesis and mechanisms of thyroid	https://pubmed.ncbi.nlm.nih.gov/23429735/
NFKB1	proliferation	Revilla et al 2019. Cross-Talk between Inflammatory Mediators	https://pubmed.ncbi.nlm.nih.gov/31109060/
NFKB2	proliferation	Revilla et al 2019. Cross-Talk between Inflammatory Mediators	https://pubmed.ncbi.nlm.nih.gov/31109060/
NOTCH1	cell differentation	Spitschak et al. 2017. MiR-182 promotes cancer invasion by link	https://pubmed.ncbi.nlm.nih.gov/28122586/
NOX4	cell growth, cell differentation	Faria et al. 2019 The Emerging Role of Estrogens in Thyroid Red	https://pubmed.ncbi.nlm.nih.gov/30728883/
NRAS	proliferation	Yoo et al. Comprehensive Analysis of the Transcriptional and M	https://pubmed.ncbi.nlm.nih.gov/27494611/
PAK4	cell growth, proliferation	Revilla et al 2019. Cross-Talk between Inflammatory Mediators	https://pubmed.ncbi.nlm.nih.gov/31109060/
PCSK2	metabolism	Rusinek et al. 2011 Gene expression profile of human thyroid ca	https://pubmed.ncbi.nlm.nih.gov/21798995/
POU5F1	cell differentation	Ahn et al. 2014. Detection of thyroid cancer stem cells in papilla	https://pubmed.ncbi.nlm.nih.gov/24302752/
PPARA	metabolism	Brocker et al. 2017. Hepatocyte-specific PPARA expression excl	https://pubmed.ncbi.nlm.nih.gov/28082284/
PPARG	metabolism	Yoo et al. Comprehensive Analysis of the Transcriptional and M	https://pubmed.ncbi.nlm.nih.gov/27494611/
PTEN	proliferation	Yoo et al. Comprehensive Analysis of the Transcriptional and M	https://pubmed.ncbi.nlm.nih.gov/27494611/
RASSF1	tumour suppressor gene	Revilla et al 2019. Cross-Talk between Inflammatory Mediators	https://pubmed.ncbi.nlm.nih.gov/31109060/
REL	proliferation	Pires et al. 2018, NF-kappaB: Two Sides of the Same Coin	https://pubmed.ncbi.nlm.nih.gov/29315242/
RELA	proliferation	Pires et al. 2018, NF-kappaB: Two Sides of the Same Coin	https://pubmed.ncbi.nlm.nih.gov/29315242/
RELB	proliferation	Pires et al. 2018, NF-kappaB: Two Sides of the Same Coin	https://pubmed.ncbi.nlm.nih.gov/29315242/
RUNX1	cell differentation	Rusinek et al. 2011 Gene expression profile of human thyroid ca	https://pubmed.ncbi.nlm.nih.gov/21798995/

S100A4	metastasis	Zhang et al. 2016. Knockdown of S100A4 blocks growth and me	https://pubmed.ncbi.nlm.nih.gov/27802204/
SLC5A5	metabolism	Yoo et al. Comprehensive Analysis of the Transcriptional and M	https://pubmed.ncbi.nlm.nih.gov/27494611/
SLC5A8	metabolism	Yoo et al. Comprehensive Analysis of the Transcriptional and M	https://pubmed.ncbi.nlm.nih.gov/27494611/
SOCS1	cell growth	Zhang et al. 2019. MiR-155 promotes anaplastic thyroid cancer	https://pubmed.ncbi.nlm.nih.gov/31718618/
SOX2	cell differentation	Pires et al. 2018, NF-kappaB: Two Sides of the Same Coin	https://pubmed.ncbi.nlm.nih.gov/29315242/
STAT1	proliferation	Rusinek et al. 2011 Gene expression profile of human thyroid ca	https://pubmed.ncbi.nlm.nih.gov/21798995/
STAT2	proliferation	Vella et al. 2018. The Emerging Role of Insulin Receptor Isoform	https://pubmed.ncbi.nlm.nih.gov/30513575/
STAT3	proliferation	Revilla et al 2019. Cross-Talk between Inflammatory Mediators	https://pubmed.ncbi.nlm.nih.gov/31109060/
STAT5B	proliferation	Revilla et al 2019. Cross-Talk between Inflammatory Mediators	https://pubmed.ncbi.nlm.nih.gov/31109060/
TG	metabolism	Giuliani et al. 2018. The Role of the Transcription Factor Nuclea	https://pubmed.ncbi.nlm.nih.gov/30186235/
TGFB1	cell growth	Revilla et al 2019. Cross-Talk between Inflammatory Mediators	https://pubmed.ncbi.nlm.nih.gov/31109060/
TGFB1I1	cell growth	Revilla et al 2019. Cross-Talk between Inflammatory Mediators	https://pubmed.ncbi.nlm.nih.gov/31109060/
TIMP3	extracellular matrix	Xing 2013, Molecular pathogenesis and mechanisms of thyroid	https://pubmed.ncbi.nlm.nih.gov/23429735/
TMEM173	innate immunity	Keskitalo et al 2019. Novel TMEM173 Mutation and the Role of	https://pubmed.ncbi.nlm.nih.gov/31866997/
TNF	apoptosis, proliferation	Pires et al. 2018, NF-kappaB: Two Sides of the Same Coin	https://pubmed.ncbi.nlm.nih.gov/29315242/
TNFRSF1A	apoptosis, proliferation	Shao et al. 2018. Associations of TNFRSF1A Polymorphisms with	https://pubmed.ncbi.nlm.nih.gov/29401539/
TPO	metabolism	Rusinek et al. 2011 Gene expression profile of human thyroid ca	https://pubmed.ncbi.nlm.nih.gov/21798995/
TRP53	apoptosis, proliferation	Yoo et al. Comprehensive Analysis of the Transcriptional and M	https://pubmed.ncbi.nlm.nih.gov/27494611/
TSHR	metabolism	Rusinek et al. 2011 Gene expression profile of human thyroid ca	https://pubmed.ncbi.nlm.nih.gov/21798995/
TYK2	proliferation	Wöss et al. 2019. TYK2: An Upstream Kinase of STATs in Cancer	https://pubmed.ncbi.nlm.nih.gov/31694222/
UHRF1	cell cycle	Rusinek et al. 2011 Gene expression profile of human thyroid ca	https://pubmed.ncbi.nlm.nih.gov/21798995/
VEGFA	proliferation, apoptosis, angioge	Revilla et al 2019. Cross-Talk between Inflammatory Mediators	https://pubmed.ncbi.nlm.nih.gov/31109060/
VIM	cytoskeleton	Faria et al. 2019 The Emerging Role of Estrogens in Thyroid Red	https://pubmed.ncbi.nlm.nih.gov/30728883/
ZEB1	cell growth	Revilla et al 2019. Cross-Talk between Inflammatory Mediators	https://pubmed.ncbi.nlm.nih.gov/31109060/